齒醫科學博士 學位論文

Study of Fibroin-Cationic Lipid Complex for Direct Intracellular Protein Delivery

피브로인-양전하 지질 복합체를 이용한 단백질의 세포 내 전달 방법에 대한 연구

2017년 2월

서울대학교 대학원

치의과학과 분자유전학 전공

김 우 진

Abstract

Study of Fibroin-Cationic Lipid Complex for Direct Intracellular Protein Delivery

WOO-JIN, KIM

Department of Molecular Genetics & Dental Pharmacology
School of Dentistry, Seoul National University
(Directed by Prof. Hyun-Mo, Ryoo, D.D.S., Ph.D.)

Directly delivering therapeutic proteins into cells has promise as an intervention without side effects for protein deficiencies caused by genetic defects. However, as negatively charged macromolecules, proteins require carriers for achieving cellular uptake and maintaining their activity in the cytoplasm. The biodegradable natural polymer silk fibroin has demonstrated outstanding advantages as a protein drug scaffold in vitro and in vivo, but its usage has been limited in the extracellular space because of its negatively charged character. Here, we present an intracellular protein delivery system based on fibroin particles coated with cationic lipid layers, denoted as

Fibroplex, the surface charge of which can be modulated. Fibroplex showed higher delivery efficiency than conventional delivery methods as well as long-term cargo release in the cytoplasm without toxicity. Furthermore, in vivo experiments showed that Fibroplex efficiently delivered tyrosinase and horseradish peroxidase, which led to hyper-pigmentation and tumor regression, respectively, suggesting its potential for therapeutic protein applications in hereditary diseases or cancer.

Pin1 is a peptidyl prolyl cis-trans isomerase that specifically binds to the phosphoserine-proline or phosphothreonine-proline motifs of several proteins. We reported that Pin1 plays a critical role in the fate determination of Smad1/5, Runx2 and β-catenin that are indispensable nuclear proteins for osteoblast differentiation. Though several chemical inhibitors has been discovered for Pin1, no activator has been reported as of yet. In this study, we directly introduced recombinant Pin1 protein successfully into the cytoplasm via fibroin nanoparticle encapsulated in cationic lipid. This nanoparticle-lipid complex delivered its cargo with a high efficiency and a low cytotoxicity. Direct delivery of Pin1 leads to increased Runx2 and Smad signaling and resulted in recovery of the osteogenic marker genes expression and the deposition of mineral in Pin1 deficient cells. These result indicated that a direct Pin1 protein delivery method could be a potential therapeutics for the osteopenic diseases.

TABLE OF CONTENTS

Ⅰ. Introduction

The intracellular modulation of key proteins is critical for treating cancer or hereditary diseases. The introduction of small-molecule chemical drugs acting as inhibitors or activators, which is a representative protein modulation method, affects diverse targets and may cause unexpected side effects[1]. Thus, using intracellular proteins as therapeutics is of great importance for achieving the direct modulation of specific disease targets with minimal side effects[2]. However, clinical applications remain rare due to not only the low cellular permeability of proteins[2-4] and the rapid degradation of unprotected proteins by extracellular and endosomal proteases but also their neutralization via binding to serum proteins, blood cells and the extracellular matrix[4]. These challenges are especially difficult in vivo[3]. While using carriers could overcome some of these problems, current methods are suboptimal.

Silk fibroin is a natural fibrous protein with a unique structure of repeating hydrophobic and hydrophilic domains that has many advantages, such as in vivo biodegradation[16]; this protein has been extensively studied for in vivo applications[17, 18]. In particular, fibroin has unique advantages for protein delivery, including a high loading capacity[19], controllable drug release kinetics[20], and the ability to encapsulate cargo proteins without covalent bonds or the use of organic solvents during fabrication[21,

22], which could disrupt the activity of the cargo proteins. Previous studies have reported the successful in vivo application of a silk fibroin scaffold for protein drugs[18, 23], but it was not for intracellular delivery, presumably because of the super-negative charge of fibroin particles[24], which inhibits cell uptake.

Cationic lipid formulations have enabled transfection with DNA or RNA to become routine techniques in basic research and have even been used in clinical trials[25]. We hypothesized that highly anionic scaffolds could be delivered via the same electrostatic-driven complexation used by cationic liposomal reagents for nucleic acid delivery. Because fibroin natively possesses the highly anionic character of nucleic acids[24], we speculated that cargo encapsulation by or noncovalent complexation with fibroin particles may produce a product that is sufficiently anionic to be efficiently delivered by common cationic lipid reagents.

In part I and II, we introduce a novel intracellular protein delivery system synergistically combined using cationic lipid encapsulation, which can be applied to the core of fibroin particles; in addition, this system exhibits controllable surface charge, which is advantageous for cellular uptake. The particle core-lipid envelope structure has high stability, low toxicity, a loading capacity and long-term release. Furthermore, this structure has shown its potential applicability by demonstrating excellent cell-introduction efficiency and long-term intracellular protein activity with model proteins, such as green fluorescent protein (GFP), horseradish

peroxidase (HRP), luciferase, and tyrosinase.

A peptidyl prolyl cis/trans isomerase (PPlase) Pin1 binds specific protein motifs and catalyzes cis/trans isomerization of the peptide bond (Yoon et al., 2013). Its association with substrates involves a WW domain that preferentially recognizes sequence motifs containing a phosphoserine or a phosphothreonine followed by a proline (pS/pT)P motif, in target substrates(Yoon et al., 2015; Yoon et al., 2013). For this reason, Pin1 frequently functions as a binary switch flipping target substrates between two states of protein structural conformations (cis or trans), thereby leading to distinct fates of the isomerized proteins by Pin1 activity. Therefore, Pin1 is associated tightly with cell signaling and Ser/Thr kinase activity as an important structural modifier (Lee et al., 2009; Ryo et al., 2003).

We previously reported that phosphorylation (Kim et al., 2004b; Lee et al., 2003) and subsequent protein stabilization of Runx2 (Jun et al., 2010; Park et al., 2010) is required for its transactivation activity for the stimulation of osteoblast differentiation. Pin1 is a critical fate determinant for the post-phosphorylation modification of Runx2 via MAPK during osteogenic cell differentiation (Islam et al., 2016; Yoon et al., 2015; Yoon et al., 2013). Thus, modifying enzymes, including Pin1, might represent valuable drug targets to correct abnormal Runx2 activity and to ensure the optimal fate determination of osteogenic cells. Previously demonstrated results suggest that an increase Pin1 level in the osteogenic cell might promote the osteogenic differentiation.

In part III, we found that recombinant Pin1 successfully encapsulated in biocompatible natural polymer, silk fibroin, and nanoparticle and delivered to various cells including Pin1-KO mouse osteoblasts (mOB). Intracellularly delivered recombinant Pin1 protein showed a controlled release pattern and maintained its activity more than 10 days with a low toxicity. These results demonstrate that increase of intracellular Pin1 protein level induce the stabilization of Runx2 and other osteogenic factors and consequently enhanced osteoblast differentiation.

Ⅱ. Part Ⅰ

Biomaterials. 2017 Jan 16;122:154-162.

Fibroin Particle-supported Cationic Lipid Layers For Highly Efficient Intracellular Protein Delivery.

Woo-Jin Kim, Bong-Soo Kim, Young-Dan Cho, Won-Joon Yoon, Jeong-Hwa Baek, Kyung-Mi Woo, Hyun-Mo Ryoo*

Department of Molecular Genetics, School of Dentistry and Dental Research Institute, BK21 Program, Seoul National University, Seoul, Republic of Korea.

Keywords:
intracellular protein delivery, fibroin, cationic lipid, protein therapy

Abstract

Directly delivering therapeutic proteins into cells has promise as an intervention without side effects for protein deficiencies caused by genetic defects. However, as negatively charged macromolecules, proteins require carriers for achieving cellular uptake and maintaining their activity in the cytoplasm. The biodegradable natural polymer silk fibroin has demonstrated outstanding advantages as a protein drug scaffold in vitro and in vivo, but its usage has been limited in the extracellular space because of its negatively charged character. Here, we present an intracellular protein delivery system based on fibroin particles coated with cationic lipid layers, denoted as Fibroplex, the surface charge of which can be modulated. Fibroplex showed higher delivery efficiency than conventional delivery methods as well as long-term cargo release in the cytoplasm without toxicity. Furthermore, in vivo experiments showed that Fibroplex efficiently delivered tyrosinase and horseradish peroxidase, which led to hyper-pigmentation and tumor regression, respectively, suggesting its potential for therapeutic protein applications in hereditary diseases or cancer.

1. Introduction

The intracellular modulation of key proteins is critical for treating cancer or hereditary diseases. The introduction of small-molecule chemical drugs acting as inhibitors or activators, which is a representative protein modulation method, affects diverse targets and may cause unexpected side effects[1]. Gene therapies introducing DNA or RNA also have limitations because many intracellular processes must occur for successful protein manifestation. In addition, this strategy presents the possibility of permanent recombination into the genome and the potential disruption of endogenous genes[2, 3].

Thus, using intracellular proteins as therapeutics is of great importance for achieving the direct modulation of specific disease targets with minimal side effects[4, 5]. However, clinical applications remain rare due to not only the low cellular permeability of proteins[2, 4-6] and the rapid degradation of unprotected proteins by extracellular and endosomal proteases but also their neutralization via binding to serum proteins, blood cells and the extracellular matrix[6]. These challenges are especially difficult in vivo[4]. While using carriers could overcome some of these problems, current methods are suboptimal. A variety of methods have been developed over recent decades to achieve intracellular protein delivery, including fusion to or conjugation with

cationic molecules that facilitate endocytosis, such as unstructured peptides[2] or engineered, super-positive proteins[7]. Proteins fused to a protein transduction peptide (PTD) have shown improved delivery efficiency[8, 9]. However, the low stability of the protein[10, 11], the low efficiency of endosomal escape[12] and the physical fusion of the PTD with the cargo protein can disrupt protein function or alter the subcellular localization of the fusion protein[13]; as a result, the amount of protein that reaches the cytosol is low, and poor biological outcomes are achieved. Other methods, such as liposomes[14], nanoparticles[6, 15] and supercharged proteins[4], have their own shortcomings, including required protein modifications[16], uncontrolled release[17] and maintenance in the cytoplasm[6], high monomer cytotoxicity[18], and low/variable delivery efficiency[19], the latter of which is perhaps the most important.

Silk fibroin is a natural fibrous protein with a unique structure of repeating hydrophobic and hydrophilic domains that has many advantages, such as in vivo biodegradation[20]; this protein has been extensively studied for in vivo applications[21-23]. In particular, fibroin has unique advantages for protein delivery, including a high loading capacity[24], controllable drug release kinetics[25], and the ability to encapsulate cargo proteins without covalent bonds or the use of organic solvents during fabrication[26-28], which could disrupt the activity of the cargo proteins. Previous studies have reported the successful in vivo

application of a silk fibroin scaffold for protein drugs[23, 29, 30], but it was not for intracellular delivery, presumably because of the super-negative charge of fibroin particles[31], which inhibits cell uptake.

Cationic lipid formulations have enabled transfection with DNA or RNA to become routine techniques in basic research and have even been used in clinical trials[32]. Notably, the fusion of liposomes with the endosomal membrane during endosome maturation can enable the efficient endosomal escape of cationic lipid-delivered cargo[33-35]. Because proteins, in contrast to nucleic acids, are chemically diverse with no dominant electrostatic property, no lipid formulation is likely to drive the efficient delivery of all proteins into mammalian cells. However, while proteins can be complexed nonspecifically and delivered by rehydrated lipids in vitro, protein complexation is dependent on high protein concentrations, is generally inefficient, and has not been widely adopted. Specialty commercial reagents developed for protein delivery have shown modest and variable efficiency with different protein cargos[4].

We hypothesized that highly anionic scaffolds could be delivered via the same electrostatic-driven complexation used by cationic liposomal reagents for nucleic acid delivery. Because fibroin natively possesses the highly anionic character of nucleic acids[31], we speculated that cargo encapsulation by or noncovalent complexation with fibroin particles may produce a product that is sufficiently anionic to be efficiently delivered by common cationic lipid reagents.

Here, we introduce a novel intracellular protein delivery system synergistically combined using cationic lipid encapsulation, which can be applied to the core of fibroin particles; in addition, this system exhibits controllable surface charge, which is advantageous for cellular uptake. The particle core-lipid envelope structure has high stability, low toxicity, a loading capacity and long-term release. Furthermore, this structure has shown its potential applicability by demonstrating excellent cell-introduction efficiency and long-term intracellular protein activity with model proteins, such as green fluorescent protein (GFP), horseradish peroxidase (HRP), luciferase, and tyrosinase.

2. Materials and Methods

2.1 Materials

All chemicals were purchased from Sigma-Aldrich unless otherwise noted and were used as received. Polyvinyl alcohol (PVA, average MW 30,000-70,000, 87-90% hydrolyzed), rhodamine B, protease XIV, horseradish peroxidase (HRP), tyrosinase (Tyr) and all other chemicals used in the study were purchased from Sigma-Aldrich (Sigma-Aldrich, USA). Enhanced green fluorescent protein (EGFP) and TAT-EGFP fusion proteins were expressed according to methods described in previous reports (Caron et al., 2001). Fusion proteins were expressed in transformed Escherichia coli BL21 and purified using a nickel-resin affinity column (Sigma-Aldrich, USA). N-[1-(2,3-Dioleoyloxy)propyl]-N,N,N-trimethylammonium methyl-sulfate (DOTAP) and 1,2-dioleoyl-sn-glycero-3-phosphoethanolamine (DOPE), and N-(7-nitrobenz-2-oxa-1,3-diazol-4-yl)dioleoyl 1,2-Dioleoyl-sn-glycero-3-phospho ethanolamine (NBD-DOPE) were purchased from Avanti Polar Lipids (Avantilipid, USA). Ultrapure water from a Milli-Q system (Millipore, USA) was used throughout this research.

2.2 Cell line cultures

The MC3T3-E1 cells were maintained in α-Minimum Essential

Medium (α-MEM), and the HEK-293, NIH3T3 and C2C12 cells were maintained in Dulbecco's modified Eagle's medium (DMEM) with 10% heat-inactivated fetal bovine serum (10% FBS) supplemented with antibiotics. Mouse embryonic fibroblasts (MEFs) were isolated from E13.5 embryos, as previously described[36]. The MEFs were grown in DMEM/10% FBS, and cells from passages 3 to 5 were used.

2.3 Preparation of fibroin particles

To prepare silk fibroin aqueous stock solutions, cocoons of Bombyx mori were boiled for 30 min in an aqueous solution of 0.02 M sodium carbonate and then rinsed thoroughly with distilled water. After air drying, the extracted silk fibroin was dissolved in 9.3 M LiBr solution at 60°C for 4 h, yielding a 20% (w/v) solution. The solution was dialyzed against distilled water using Slide-A-Lyzer Dialysis Cassettes (MWCO 3500, Pierce, USA) for 3 days to remove the salt. The solution was centrifuged 2 times at 10,000 rpm for 20 min to remove silk aggregates as well as debris from the original cocoons. The final concentration of the silk fibroin aqueous solution was approximately 8% (w/v), based on weighing the residual solid of a known volume of solution after drying at 60°C. The 8% silk stock solution was stored at 4°C and diluted with ultrapure water before use. Silk and PVA stock solutions were prepared at a concentration of 5 wt%. Blending was performed by

gently mixing the silk and PVA stock solutions. To obtain a blend with a 5 wt% final solute concentration and a silk/PVA weight ratio of 1/4, 1 ml of the 5 wt% silk solution was mixed with 4 ml of the 5 wt% PVA solution. The blended solutions were then subjected to sonication using a Vibra Ultrasonicator (VCX130, Sonics, USA) at an energy output of 30% amplitude for 30 s in an ice box to prevent heat damage. The solution was immediately transferred to open 100x15 mm diameter petri dishes after sonication and dried overnight. The films of the dried silk/PVA blend prepared from blended solutions were dissolved in 30 ml of ultrapure water in 50 ml centrifuge tubes with 10 min of gentle shaking at room temperature. The tubes were centrifuged in a centrifuge (5810R, Eppendorf, Germany) at 14,000 rpm and 4°C for 30 min. The supernatant was carefully collected for analysis, and the pellet was suspended in 30 ml of ultrapure water and centrifuged again. The final pellet was suspended in 2 ml of phosphate-buffered saline (PBS) and sonicated at 10% amplitude for 15 seconds with the ultrasonicator to disperse the clustered particles.

2.4 Loading fibroin particles with protein

EGFP, HRP, Tyr and luciferase (Luc) were used as model drugs to study fibroin particle drug loading. Stock solutions with a concentration of 500 μM in PBS buffer, pH 7.4, were first prepared and stored at −20°C. Before loading, certain amounts of the stock

solutions were added to the silk solutions to reach a drug : silk volume ratio of 1:9. After mixing, the solution was blended with the PVA solution following the steps described for the fibroin particle preparation. A 5 wt% polymer concentration and silk : PVA ratio of 1:4 was used in this study. To determine protein loading in the silk spheres, the supernatants collected from the centrifugation steps were analyzed by ELISA. The amount of protein was calculated based on a standard curve obtained under the same conditions. The amount of protein loaded onto the fibroin particles was calculated from the difference between the total amount used and the amount remaining in the supernatants. For each drug loading, at least three samples were prepared to obtain a standard deviation. The pellets from the last centrifugation step were suspended in PBS buffer, pH 7.4, and used for subsequent studies.

2.5 Preparation and characterization of Fibroplex

Fibroplex was formed by fusing cationic lipids with silk fibroin particle cores, and the proportion of cationic lipids was optimized to maintain the biocompatibility of Fibroplex. Fibroplex were formed by cationic liposomes to the fibroin particle core as reported previously [37]. In detail, fibroin particles are prepared per unit weight and then dispersed by weak sonication at 10% amplitude (VC-130, Sonics, USA) for 30 seconds in 4 ℃ PBS. After particle dispersion, cationic lipids according to each weight ratio are mixed with fibroin

particle solution and then vortexed for 30 seconds at room temperature. Fibroin particles and cationic lipids interact spontaneously when incubated for 30 min at room temperature. Excess lipid is removed via light centrifugation before use. Cationic lipids (DOTAP) with 1:1 w/w PE (DOPE) were used in all further studies and were expected to be coated on the outer surface of the fibroin particle core. As a fluorescence label for cationic lipid membranes, 0.1 wt% 7-nitrobenzofurazan-labeled DOPE (NBD-DOPE) was used to study the membrane structure of Fibroplex.

Scanning electron microscopy (SEM) images were obtained with a Hitachi S-4700 field-emission instrument. Dynamic light scattering (ELSZ 1000, Photal Otsuka electronics, Japan) was used to determine the hydrodynamic size and zeta potential of Fibroplex.

2.6 Drug release from Fibroplex

Fibroplex loaded with the model drugs was suspended in 1 ml of PBS buffer, pH 7.4. The samples were incubated at 37°C under slow shaking. At certain time points, samples were centrifuged at 16,000 rpm for 10 min with a microcentrifuge (5417R, Eppendorf, Germany), the supernatants were carefully transferred to empty tubes, and the pellets were suspended in 1 ml of PBS buffer to continue the release study. The absorbance of the collected supernatants was then measured at 555 nm. The amount of model drug was then calculated based on a standard curve. The cumulative

release was obtained by comparing the data with the original extent of sphere loading. For each model drug, at least three samples were prepared to obtain statistical data.

2.7 In vitro cellular delivery assay

The results of cellular internalization studies were assessed via confocal laser microscopy (CLM) and fluorescence-activated cell sorting (FACS). MC3T3-E1 cells were cultured in α-MEM supplemented with 10% FBS and 1% penicillin/streptomycin. Cells (1.5×10^6 cells/100 mm plate) were seeded the day before Fibroplex was added. Fibroplex and fibroin particles loaded with equal protein concentrations were added to the cell medium. After incubation at 37°C for 12 h, the cells were washed three times with PBS containing heparin sulfate (40 μg/ml) to remove free particles. Then, the cells were incubated for an additional 24 or 48 h and either visualized with by CLM or trypsinized, centrifuged, re-suspended in PBS and analyzed via FACS. The actin staining was performed according to manufacturer's instructions. Briefly, after incubation with Fibroplex, cells were briefly washed, fixed with 2% formaldehyde, stained with rhodamine-phalloidin for 10 min, and then observed by CLM.

2.8 Cytotoxicity assay

The toxicity of the Fibroplex was assessed by the MTT assay. MC3T3-E1 cells (7,000 cells/well) were seeded on a 96-well plate the day prior to Fibroplex exposure. Different concentrations of Fibroplex were incubated with the cells for 12 h; subsequently, the cells were incubated with fresh media for different times. Cationic lipids (1:1 wt% DOTAP:DOPE) and fibroin particles were treated as controls. MTT solution (20 μl) was added to each well and incubated for 3 h. The medium was then removed, and 100 μl of DMSO was added to the cells. The plate was placed on a shaker table for 5 min at 150 rpm to thoroughly mix the solution, and then the absorbance was measured at 560 nm. Untreated cells were used as the 100% cell proliferation control.

2.9 Endocytosis inhibition

MC3T3-E1 cells (30,000 cells/well, 24-well plate) were seeded the day prior to the addition of Fibroplex. Before the experiment, the medium was replaced with 0.5 ml of fresh medium with 10 μg/ml nocodazol (ND, inhibitor of macropinocytosis), 10 μg/ml chlorpromazine (CPZ, inhibitor of clathrin-mediated endocytosis), or 30 μg/ml nystatin (Nys, inhibitor of caveolae-mediated endocytosis). After 30 min, 120 nM EGFP-loaded Fibroplex was added to the medium, and the cells were incubated at 37°C for 12 h. After being washed with PBS containing heparin sulfate, the cells were trypsinized, centrifuged, re-suspended in PBS and analyzed via

FACS. Cells incubated at 37°C and 4°C in medium without endocytosis inhibitors were used as positive and negative controls, respectively.

2.10 In vivo evaluation of Fibroplex uptake

All animal experiments were conducted after obtaining the approval of the Seoul National University Institute of Laboratory Animal Resources and Use Committee. Each of the C57BL/6 mice (Orient Bio., Kyungi, Korea), 6-8 weeks old, was subcutaneously injected with 150 μl of a Fibroplex saline solution, a fibroin particle saline solution, or a saline solution (control). After 3 or 7 days, the mice were sacrificed, and the skin and all major organs were excised for ex vivo imaging. Then, the frozen organs were embedded in a freezing medium, and cryosections were prepared using a microtome. The tissue sections containing Fibroplex were stained with both DAPI (for nuclei) and dihydroethidium for HRP and then observed by CLM.

2.11 Subcutaneous tumor regression

Female, 4-week-old C57BL/6 mice were obtained from Orient Bio. (Orient Bio, Korea) and kept under sterile conditions. To establish tumors, B16-F10 tumor cells (1×10^7) suspended in 150 μl of saline were subcutaneously inoculated in the left ventral

abdomen and incubated for 20 days. When the tumor volume reached 200−300 mm^3, the tumor−bearing mice were subjected to an in vivo HRP delivery study. For the HRP transfection assay, 150 μl of HRP−loaded Fibroplex (1 μM) was subcutaneously injected into the tumor area. Indole−3−acetic acid (IAA) was then injected into the intraperitoneal space. Tumor measurements were made daily in three dimensions using calipers, and the tumor volume was calculated using the following formula: V = (a*b*c*pi)/6.

2.12 Melanoma cell growth inhibition assay

B16−F10 melanoma cells placed in 96−well plates (3,000 cells/well) were incubated with HRP−loaded Fibroplex, fibroin particles or native HRP for 12 h; after being washed, the cells were exposed to different concentrations of IAA for 24 h. The half maximal inhibitory concentration was determined from the cell viability curve determined using MTT.

2.13 Statistical Analyses

The quantitative data are presented as the mean ±S.D. Each experiment was performed at least three times, and the results from one representative experiment are shown. Statistical differences were analyzed by Student's t test. A p value of statistical significance was mentioned in the individual figure legend.

3. Results and Discussion

As illustrated in Fig. 1a and demonstrated by previous studies[27, 31], fibroin can be formed into spherical particles using polyvinyl alcohol and ultrasonic energy, and these particles can be loaded with various cargos without additional covalent bonds. These fibroin particles have an anionic electrostatic charge of −21.13 ± 4.78 mV, which was found to be independent of cargo type (Supplementary Table S1). However, the fibroin particle−lipid complexes had stable positive charges; moreover, the surface charge could be adjusted to a certain degree by controlling the mixing ratio of the lipids and particles. We denoted this particle−lipid complex as Fibroplex, and Fibroplex loaded with enhanced green fluorescent protein (EGFP), HRP, luciferase, or tyrosinase was referred to as Fib(GFP), Fib(HRP), Fib(Luc), and Fib(Tyr), respectively.

Structurally, Fibroplex comprises a thin lipid layer that strongly interacts with the fibroin particle surface. As expected, scanning electron microscopy (SEM) images of Fibroplex showed a thin layer surrounding the fibroin particle surface (Fig. 1b). Similar results were also found when Fibroplex was formed with 7−nitrobenzofurazan (NBD)−labeled cationic lipids and rhodamine B−labeled fibroin particles; observation by confocal laser microscopy (CLM) showed a green, ring−like layer coating the red particle core. Moreover, three−dimensional (3D) images reconstructed from

Z axis sections also confirmed that the Fibroplex structure consisted of lipids layers encapsulating fibroin particles (Fig. 1c).

The negatively charged fibroin particles became positively charged when in the form of Fibroplex, and this tendency could be modulated by changing the weight ratio of the lipid and fibroin particles. The zeta potential analysis revealed that the native fibroin particles had a highly negative electrostatic charge, as previously reported[31]; however, upon being coated with a cationic lipid layer, the potential dramatically shifted to more positive values, which ranged from −6.7 to +27.2 mV with different weight ratios. This charge shifting tendency was also observed by CLM. Therefore, the hyper−anionic charge of Fibroplex caused by particle−lipid complexation can be used to control transfection efficiency and reduce unexpected cationic lipid toxicity due to over treatment. In fact, cationic delivery systems are often toxic when delivered in high concentrations; however, when we performed an MTT assay, even high concentrations of Fibroplex showed low cytotoxicity (Supplementary Fig. S1).

Structurally, Fibroplex remained stable for 70 days at 37°C in serum, as revealed by CLM images. Zeta potential changes in serum were also evaluated. The zeta potential of cationic liposomes rapidly decreased to undetectable (null) values within 7 days, indicating that the measurable structures were disrupted; however, Fibroplex showed only a 15% decrease in zeta potential from the initial value over 70 days, indicating that the Fibroplex structure was stably

maintained. In addition, there was no difference between the cellular uptake efficiency of Fibroplex at 10 days or immediately after complex formation (Fig. 1d).

We first tested whether the negatively charged fibroin particles could mediate the complexation and delivery of loaded cargo. As illustrated in Fig. 2a, most of the MC3T3-E1 cells treated with Fib(GFP) showed strong fluorescence, while cells that had been treated with only naive GFP (data not shown) or GFP-loaded fibroin particles [(Par(GFP)] showed no or low fluorescence. A 3D analysis with actin staining was conducted to investigate the intracellular particle distribution and revealed that most of the EGFP that had been taken up by the cells was in the cytosol near the nucleus.

The cellular uptake of Fibroplex exhibited superiority in both efficiency and quantity. At the same protein concentration, cells incubated with Fib(GFP) (loaded with 150 nM EGFP) showed higher fluorescence intensities than those incubated with conventional delivery systems, i.e., EGFP fused with a TAT sequence (CPP) or commercial protein transfection reagent (PTR; Pro-Ject, Thermo Fisher). Fluorescence-assisted cell sorting (FACS) analysis revealed that the CPP and PTR systems led to 64% and 82% of the cells exhibiting detectable fluorescence; however, 97% of the cells incubated with Fib(GFP) exhibited detectable fluorescence, which indicated that Fib(GFP) had a relatively higher transduction efficiency (Fig. 2b). According to the mean fluorescence intensity,

which represents the amount of EGFP in a cell, Fibroplex showed approximately 32- to 49-fold higher EGFP concentrations than PTR or CPP (Supplementary Fig. S2). When large amounts of protein are present in cells, the excess may cause endoplasmic reticulum (ER) stress. However, after treating MC3T3-E1 cells with Fib(GFP), the expression levels of ER stress-related markers were minimal, suggesting that low ER stress occurred despite the high protein concentration introduced (Supplementary Fig. S3).

In addition, Fibroplex was advantageous in terms of being applicable to various cell types and delivering multiple types of cargo. FACS analysis was conducted on different cell types that were treated with PTR(GFP), Par(GFP) or Fib(GFP), and the results showed great differences in delivery efficiency. In each group, only approximately 1-7% of the cells that had been treated with Par(GFP) generated fluorescence. The PTR(GFP)-treated cells showed relatively higher rates, ranging from 39-84%, while the cells that had been treated with Fib(GFP) showed consistently higher uptake rates. Specifically, 99% of NIH3T3 and MC3T3-E1 cells and 92% of HEK293 cells generated fluorescence; Fibroplex could deliver EGFP into various cell types, including cancer and primary cells, with consistently high efficiency (Fig. 2c). Furthermore, successful cell uptake and cargo release was achieved with Fibroplex simultaneously loaded with both bovine serum albumin and dextrin, thereby demonstrating the delivery of multiple cargo types.

Fibroplex could even effectively deliver large enzymes, such as HRP, luciferase and tyrosinase, which then exhibited stable enzymatic activity in the cytoplasm. Luciferase is a useful tool for intracellular enzymatic assays because of its large size and complicated properties that prevent it from moving freely across the cellular membrane. Recombinant luciferase was successfully encapsulated by fibroin particles. Moreover, when MC3T3-E1 cells were treated with Fib(Luc), the intracellular concentration of luciferase increased proportionally with the amount of Fib(Luc). After cells were treated with naive luciferase or Par(Luc), no enzymatic activity could be detected; in contrast, when cells were treated with Fib(Luc), they displayed very high luciferase activity, and the luminescence was directly proportional to the amount of Fibroplex administered (Fig. 2d).

As a key enzyme for melanin synthesis, tyrosinase is a therapeutic target in hereditary disorders associated with skin pigmentation and has also recently been proposed as a potential diagnostic imaging tool for cancer[38]. As shown in Fig. 2e, cells treated with Fib(Tyr) produced pigment at a level similar to that of B16F10 melanoma cells. In addition, after being complexed with fibroin particles, HRP remained active for more than six months at 37°C (data not shown), and we observed that cells treated with Fib(HRP) accumulated dye when treated with the chromogenic substrate 3,3,5,5-tetramethylbenzidine (TMB; Fig. 2f).

Cellular uptake can occur through a variety of pathways, which

determine the fate of cargos in the cytoplasm. Co-localization with LysoTracker staining was used to verify that Fibroplex is transported into cells via endocytosis (Fig. 3a). To identify the specific endocytosis pathway involved, we treated cells with endocytosis pathway-specific inhibitors. The successful endosomal escape demonstrated in previous study [35], As shown in Fig. 3b, caveolae- or clathrin-mediated endocytosis is thought to be involved in Fibroplex cellular uptake, and these pathways have been reported to have a high possibility of endosomal escape. Optimal pH response and protectivity is essential for endocytotic delivery of cytoplasm[39]. Fibroplex could also protect cargo against pH shock and proteases during the process of endosomal transport, which can have significant effects on the activity of cargo proteins (Supplementary Figs. S4 and S5).

Fibroplex showed a stable sustained release profile in serum. We investigated the cumulative release patterns of fibroin particles, Fibroplex, and PTR and found that Fibroplex showed sustained release profiles, with approximately 60% release of loaded protein occurring over 100 days; in contrast, the liposome-based PTR released GFP over 5 days, and the GFP protein activity was depleted after 11 days (Fig. 3c). The molecular characteristics of cargos were found to exert significant effects on the release pattern of Fibroplex. Over a period of 63 days, 34-54% release was observed from Fibroplex loaded with GFP, HRP, and dextran, which are charged hydrophilic molecules. On the contrary, the maximum

release of fluorescein isothiocyanate (FITC) and rhodamine B, which are relatively small and hydrophobic molecules, was 11% over the same period. The silk fibroin is a protein composed of repeated sequences of hydrophobic amino acids[40]. Therefore, silk fibroin particles are believed to bind strongly to hydrophobic or positively charged molecules as described previously[31]. Fibroplex showed an effective and selective release profile for proteins (Fig. 3d). The stable, sustained release profile of Fibroplex for protein drugs also resulted in long-term intracellular protein activity. We treated cells with Fib(GFP) and observed the cells for 10 days; the maximum EGFP activity was observed at 4-5 days, and the fluorescence was maintained continuously until after 10 days. This release pattern associated with cytoplasmic component affects the stability of EGFP, and as a result, the fluorescence that appears in the cell means the amount of cargo present at that moment rather than cumulated cargo. The same release profile was also observed when HRP was delivered into the cells (Figs. 3e and 4f).

To confirm the efficiency of Fibroplex transport and biodistribution in vivo, we subcutaneously injected Fibroplex into the dorsal skin of mice. At 7 days after injection, intense fluorescence was detected in the skin layers, and significantly greater fluorescence was observed after treatment with Fibroplex than with the controls. Similar distributions and enzymatic activity levels were observed in tissue cross-sections from the Fib(HRP)- and Fib(GFP)-treated groups. The in vivo toxicity of Fibroplex was

examined in kidney, liver and spleen tissues of mice 1 day and 4 weeks after Fibroplex injection. Histopathologically, no significant toxicity was observed in these tissues relative to the controls (data not shown).

Protein therapies using tyrosinase have been attempted to be used for treating hereditary disorders, such as vitiligo[41], and the accumulation of nontoxic natural pigments in cancer is considered as an important diagnostic tool. However, the delivery of tyrosinase into the cytoplasm has been very challenging. To investigate the possibility of delivering tyrosinase into skin tissue in vivo using Fibroplex, we subcutaneously injected Fib(Tyr) into the dorsal area, and we observed the formation of black spots around the injection site (white dotted circle) after 15 days (Fig. 4a). As shown in Fig. 4b, melanin accumulation was not observed in histological sections from the Par(Tyr)-treated group, as in normal skin; however, in the Fib(Tyr)-treated group, melanin accumulation was observed in all skin layers. The melanin pigmentation was more prominent in the epidermis and muscle layers, which have high cell densities; upon magnification (dotted line area), melanin accumulation was observed in each area from the muscle fibers to the upper layer of the epidermis (black arrows). A Western blot analysis was conducted to detect tyrosinase in each tissue sample, and we also observed a strong tyrosinase band (120 kDa) only in the Fib(Tyr)-treated group (Supplementary Fig. S6).

The ability to deliver active proteins with high efficiency,

long-term stability and low toxicity opens new possibilities for cancer therapies[42]. The combination therapy of HRP with indole-3-acetic acid (IAA), a nontoxic vegetable hormone, has been highlighted as an effective gene therapy for such cancers as melanoma[43], transporting HRP into cancer cells and achieving HRP expression remain difficult tasks[44]. In this context, we first confirmed in vitro that the viability of B16F10 melanoma cells treated with Fib(HRP) decreased significantly with increasing IAA concentrations. Then, we evaluated the anti-cancer potential of Fib(HRP) in vivo. For tumor formation, B16F10 cells were subcutaneously implanted into the lateral ventral area of mice and allowed to grow for 20 days. After the formation of tumor-bearing mice, we subcutaneously injected Fib(HRP) with IAA and observed subsequent changes in tumor volume for 21 days. The average initial tumor volume was 261.12 ± 34.24 mm^3, and in the control group, the tumor volume increased 1.87-fold over 21 days. There were no significant differences in tumor volume between the sham treatment and treatment with IAA or Fibroplex alone. However, in mice co-treated with IAA and Fib(HRP), the tumor volume was reduced by 87% to a mean volume of 38.31 ± 12.24 mm^3 (Figs. 4c and 4d), and significantly decreases were observed in the number of blood vessels connected to the tumor mass, indicating reduced tumor vascularity (Fig. 4c, black arrow).

4. Conclusion

These results show that Fibroplex can be fabricated with natural silk fibroin protein and clinically applicable cationic lipids to achieve high intracellular delivery efficiency with enhanced capacity and stability. Fibroplex showed supreme biocompatibility and protected cargos from being damaged during endocytosis, enabling the stable, long-term, intracellular release and activity of cargos. As a result, more therapeutic proteins could be delivered into cells, and the successful delivery of functional proteins into tissues in vivo suggests the possibility of using Fibroplex for delivering protein drugs in clinical applications.

Fibroplex provides an alternative method for delivering proteins more effectively. We were able to deliver various proteins into skin tissue, and we observed long-term, stable protein delivery followed by protein activation, which could facilitate the application of therapeutic proteins in treating hereditary diseases or cancer. As such, we expect that by modifying the cationic lipids with disease-specific ligands [45, 46] and confirm the bio-distribution of Fibroplex via intravenous injection, we will be able to deliver proteins into specific target tissues or cells and deliver multiple proteins that simultaneously regulate cellular functions. Such a novel intracellular protein delivery system will provide opportunities for the use of protein drugs in cellular imaging applications and in therapies for cancer and hereditary disorders.

Fig. I-1

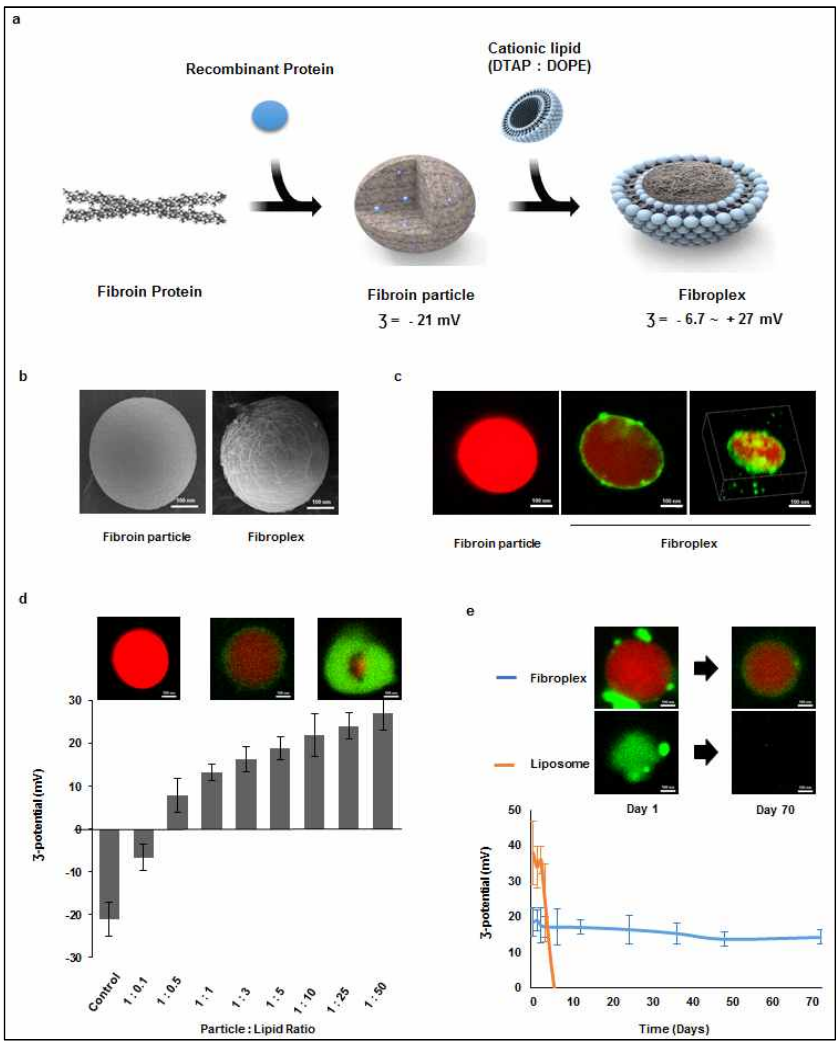

Figure I-1. Strategy for delivering proteins into mammalian cells by complexation with anionic fibroin particles and complexation with cationic lipids.

(a) The crystalline nature of silk fibroin particles facilitated the entrapment of proteins of different molecular weight and hydrophobicity, resulting sustained drug release and protection from the harsh in vivo environment. Through a simple sonication and

drying process, the aqueous fibroin protein solution efficiently formed spherical fibroin particles, which show a highly anionic electrostatic character (−21 mV). When these particles were complexed with cationic lipids at various weight ratios, they formed a stable interaction with a controllable cationic surface charge ranging from −6.7 to +27.2 mV. (b) The SEM images show that the fibroin particle and lipid complexes consist of thin (>5 nm), homogenous layers of lipids coating the core of the fibroin particles. Scale bars represent 100 nm. (c) Fibroin particles were loaded with rhodamine B (RhB, Red) and supported by NBD−labeled cationic liposomes (Green). CLM imaging revealed the resulting complex (called "Fibroplex") that exhibited a green ring around a red spherical core. Scale bars represent 100 nm. (d) Correlation between the surface charge and core particle/cationic lipid weight ratios. The fibroin particle concentration was fixed at 3 μg/ml, and the cationic lipid concentration was increased from 0.3 to 150 μg/ml. Each CLM image shows a specific particle/lipid ratio; Control (right), 1:2 (middle) and 1:50 (left). (e) The structural stability was increased by the lipid−particle interaction. Fibroplex (blue bar) or liposomes (orange bar) were incubated with 100 wt% fetal bovine serum at 37°C. The CLM images showed that the initial lipid−coated structure of Fibroplex was maintained for 70 d, while the liposomes disintegrated in 5 d. All error bars reflect the standard deviation of three independent biological experiments performed on different days.

Fig. I-2

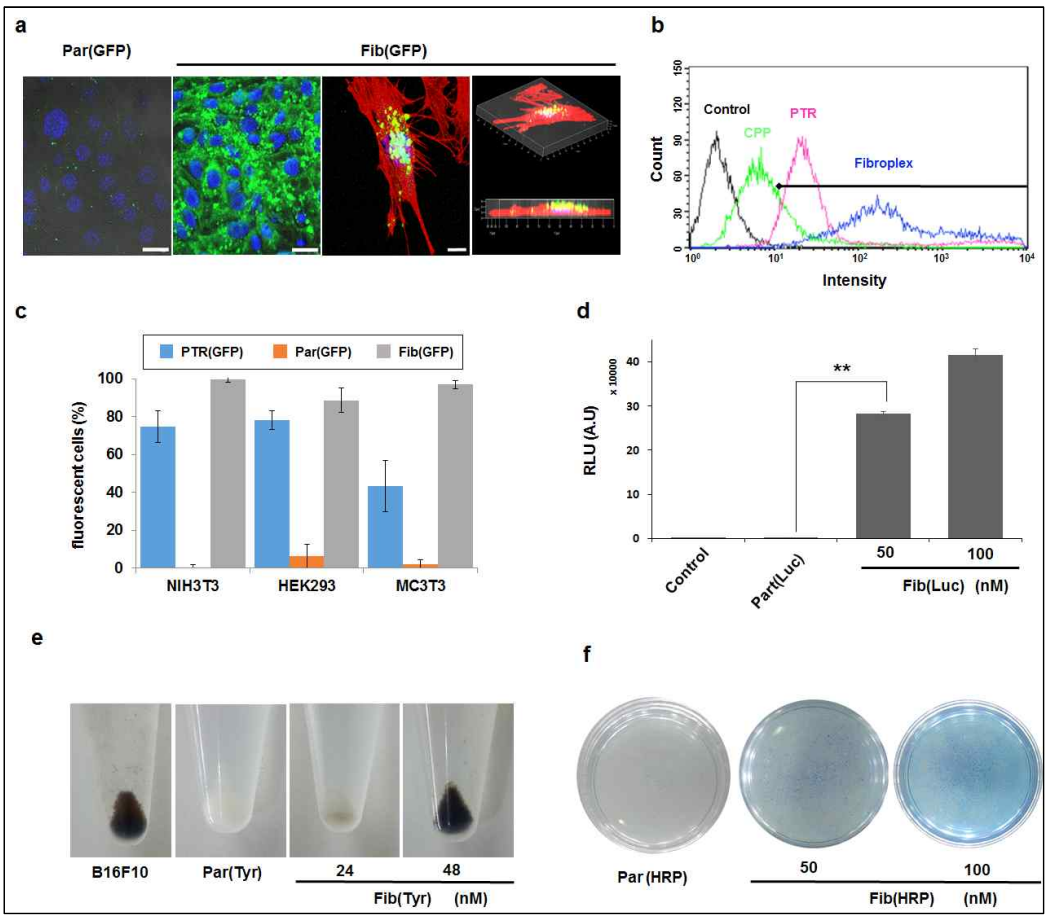

Figure I-2. Fibroplex delivered recombinant proteins into the cytoplasm with high efficiency.

(a) CLM images showing the delivery of Fib(GFP) but not of Par(GFP). MC3T3-E1 cells were treated with Fib(GFP) or Par(GFP) loaded with 150 nM GFP; the same particle cores were used, the and Fibroplex was produced at a 1:1 lipid:particle wt ratio. Cells were visualized with DAPI (for nuclei) after 48 h of treatment. Cells were counter-stained with rhodamine-phalloidin

(for F-actin) to identify the cell boundaries. All scale bars represent 10 μm. (b) FACS analysis of MC3T3-E1 cells incubated with 150 nM EGFP for 48 h via different delivery systems, i.e., TAT-EGFP fusion proteins (CPP), commercial PTR or Fibroplex. (c) Comparison of delivery efficiency in different mammalian cells. All cells were incubated for 48 h with PTR, fibroin particles, or Fibroplex, all loaded with 150 nM EGFP. (d) Relative catalytic activity of luciferase after transduction with Par(Luc) or Fib(Luc) at different concentrations. MC3T3-E1 cells treated with fibroin particles and Fibroplex loaded with 50 and 100 nM luciferase. Each sample was incubated for 12 h, washed 3 times to remove free proteins, and then incubated for an additional for 48 h before the luciferase assay was performed. (n = 3) (e) Pigmentation of transfected mouse calvarial cells. MC3T3-E1 cells were incubated with Fib(Tyr) for 120 h after free tyrosinase was removed. The induced black pigmentation visible in the cell pellet intensified with increasing Fib(Tyr) concentrations. (f) MC3T3-E1 cells were incubated with Par(HRP) or Fib(HRP) for 72 h after free HRP was removed. The cells were then and incubated with the chromogenic HRP substrate TMB for 10 min. All error bars reflect the standard deviation of three independent biological experiments performed on different days (**$p < 0.001$, by the t-test).

Fig. I-3

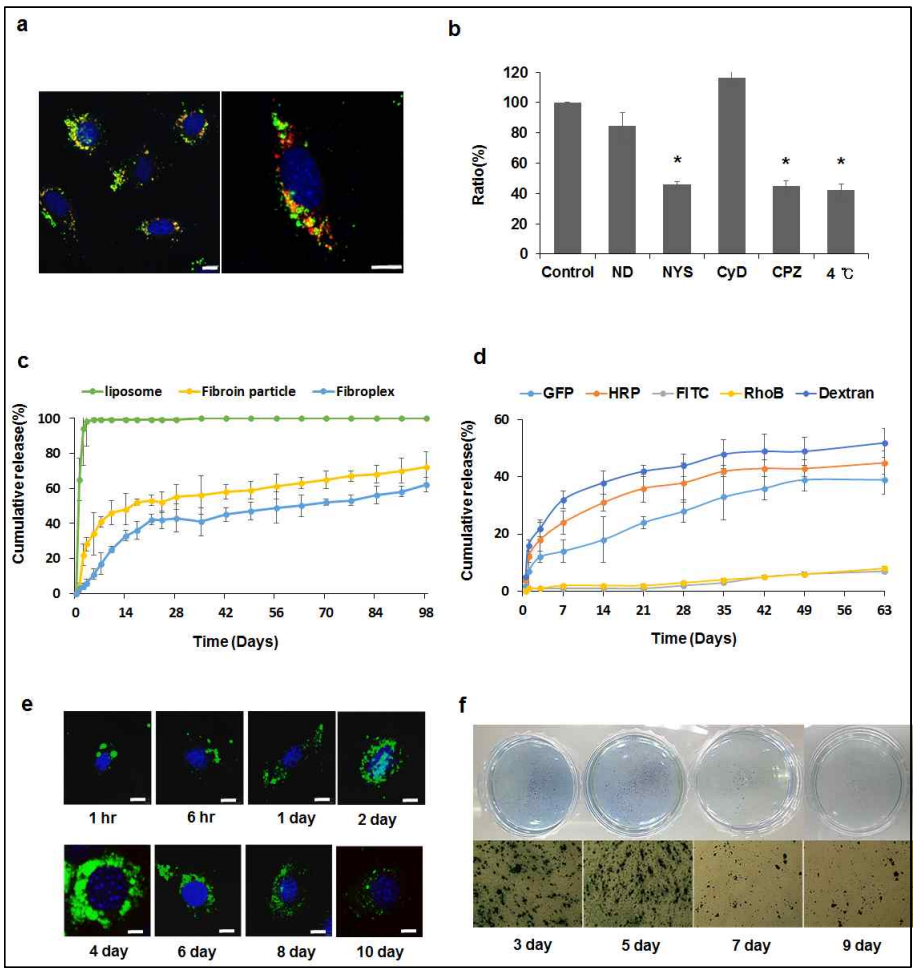

Figure I-3. Fibroplex penetrated the cell membrane via endocytosis and allowed the sustained released of protein cargos.

(a) LysoTracker staining and the intracellular distribution of Fib(GFP). After 12 h, some green fluorescence of GFP co-localized with late endosomes (Red) appeared as yellow florescence around the nuclei, and some green fluorescence was observed in the cytoplasm. Cells were incubated with Fibroplex loaded with 150 nM EGFP and visualized with DAPI and LysoTracker-RED after

fixation. (b) Fibroplex was internalized both by clathrin- and caveolae-mediated endocytosis. For the inhibition of endocytosis, samples were pretreated with 10 μg/ml nocodazole (Noc), cytochalasin D (Cyt D) and chlorpromazine (CPZ) and 25 μg/ml nystatin (Nys) for 30 min, followed by 12 h of incubation with Fib(GFP). The effect of each inhibitor was evaluated by monitoring the internal fluorescence by FACS. Cell viability was >90% with each inhibitor treatment, as determined by trypan blue staining. (n = 3) (c) Cumulative protein release profiles of Fib(GFP) and PTR(GFP) incubated in serum at 37°C, pH 7.4. Each sample was incubated for multiple time periods, centrifuged to remove free proteins, and analyzed by ELISA. (d) Cumulative release of Fibroplex loaded with various model drugs showing stable release profiles for hydrophilic macromolecules, i.e., proteins and saccharides, as determined by measuring the amount of drug present in the supernatant fraction after centrifugation. (e) CLM images of MC3T3-E1 cells after 10 days of treatment with Fib(GFP). (f) MC3T3-E1 cells after incubation with Fib(HRP) for 10 days. TMB was administered at specific time points and incubated with the cells for 30 min. Chromogenic reactions were visualized as blue dots (upper), and magnified images (40x) also showed intracellular pigment deposition at the same time points (lower). All scale bars represent 10 μm, and all error bars reflect the standard deviation of three independent biological experiments performed on different days (*$p < 0.05$, by the t-test).

Fig. I-4

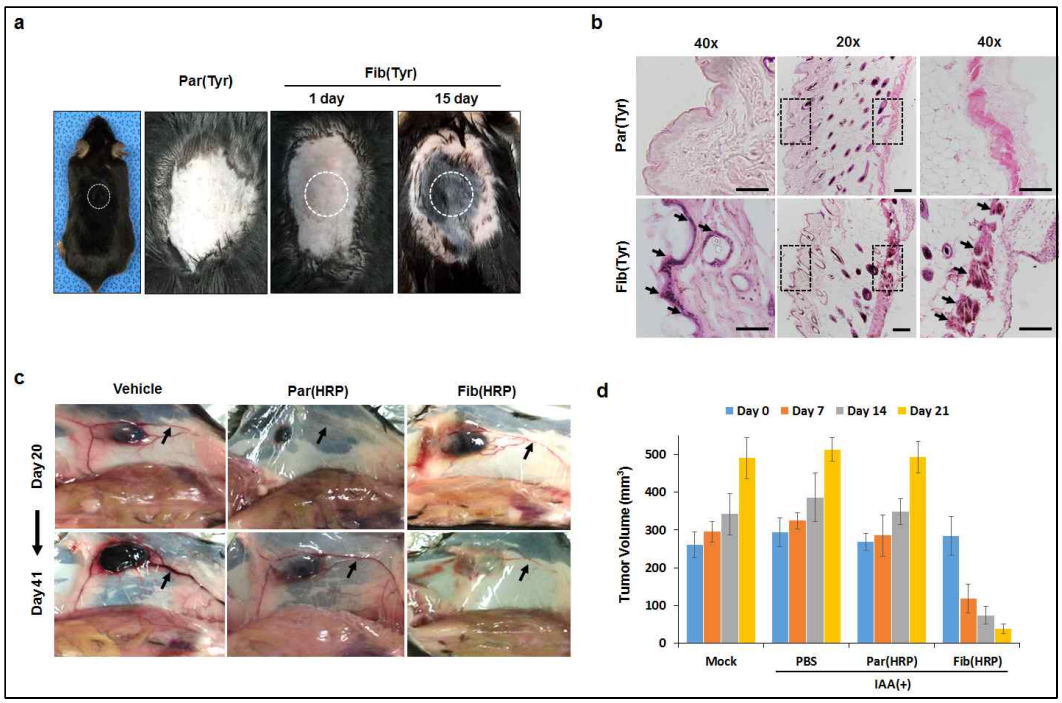

Figure I-4. In vivo delivery of therapeutic targets using Fibroplex. (a) Images of dorsal skin tissue of mice treated with Fib(Tyr) for 15 days. The shaved dorsal skin of each 6- to 8-week-old mouse was subcutaneously injected with Fib(Tyr) or Par(Tyr) loaded with 1 μM tyrosinase in 150 μl of saline. (b) Hematoxylin and eosin staining of mouse skin sections collected 15 days after subcutaneous injection. The black box shows high melanin pigment deposition in the superficial layer and basal area of the skin, which are shown separately in magnified images (40x). Scale bars represent 100 μm. (c) Representative images of tumor-bearing mice 21 days after treatment. Co-treatment with Fib(HRP) and IAA significantly reduced tumor volume, and the black arrow indicates

tumor-connected blood vessels. (d) B16F10 cells were implanted in C57BL6 mice, which were then treated with Fib(HRP), Par(HRP) or vehicle(PBS) solution (control) and 200 mg/kg IAA for 21 days starting on day 20 after tumor cell inoculation. Fib(HRP) and IAA treatment inhibited melanoma growth. The mean tumor volumes (n=5) on the day of sacrifice are indicated with the standard deviation.

Supporting Informations

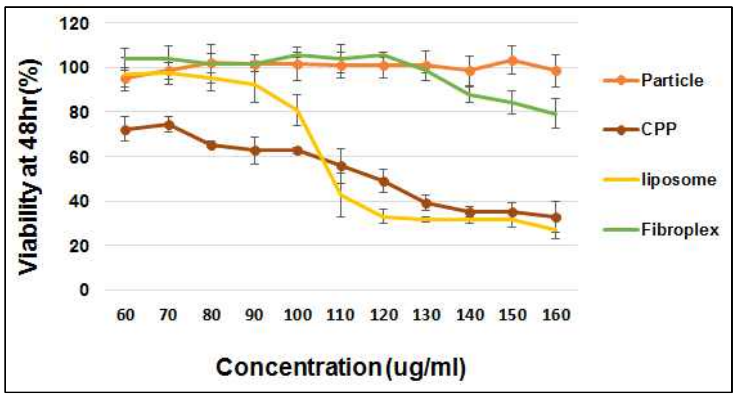

Supplementary Figure S1. MTT assay results showing MC3T3-E1 cell viability after treatment with different concentrations of EGFP fused with a TAT sequence (CPP), protein transfection reagent (PTR) and Fibroplex for 48 h. Fibroplex and fibroin protein exhibited a cytotoxicity similar to that of untreated cells, but cells treated with CPP and PTR were 50% viable at a concentration of approximately 100 μg/ml. The cell proliferation rates were normalized to those of untreated cells.

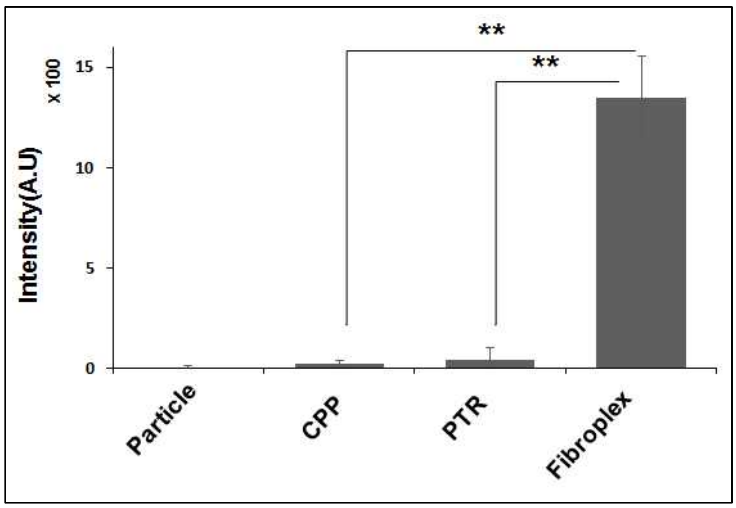

Supplementary Figure S2. In Vitro delivery efficiency of Fibroplex. Y-axis reveals luciferase activity via luciferase assay (Promega, USA).

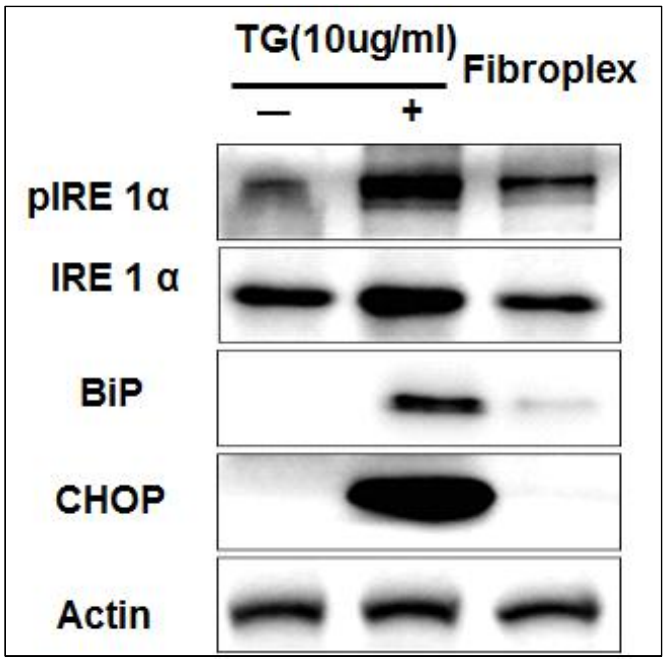

Supplementary Figure S3. Western blot analysis for endoplasmic reticulum stress and unfolded protein response due to treatment with Fibroplex. Subconfluent cultures of MC3T3-E1 cells were incubated with 150 nM of Fib(GFP) for 48 h, and control cells were treated with 10 μg/ml thapsigargin (TG). Detergent lysates were prepared and analyzed by Western blot with anti-phospho-IRE 1α, anti-BiP and anti-CHOP antibodies. Blots were re-probed with anti-β-actin antibodies to confirm equal protein loading.

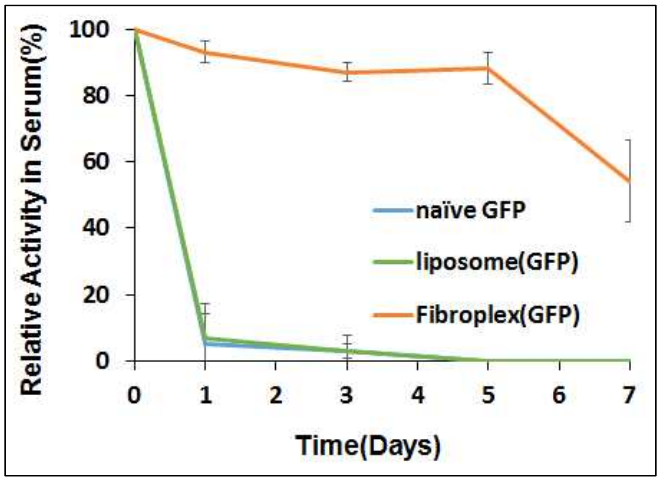

Supplementary Figure S4. Fibroplex showed an outstanding ability to protect the activation of the encapsulated protein drug. Fluorescence measurements showed that in an environment similar to blood (37°C with FBS and a low concentration of trypsin), 150 nM naive GFP maintained only 3% or less of the protein structure within 24 h (generated fluorescence), whereas, under same conditions, Fibroplex showed a 10% decrease in fluorescence over 5 days and maintained 37% fluorescence for up to 10 days.

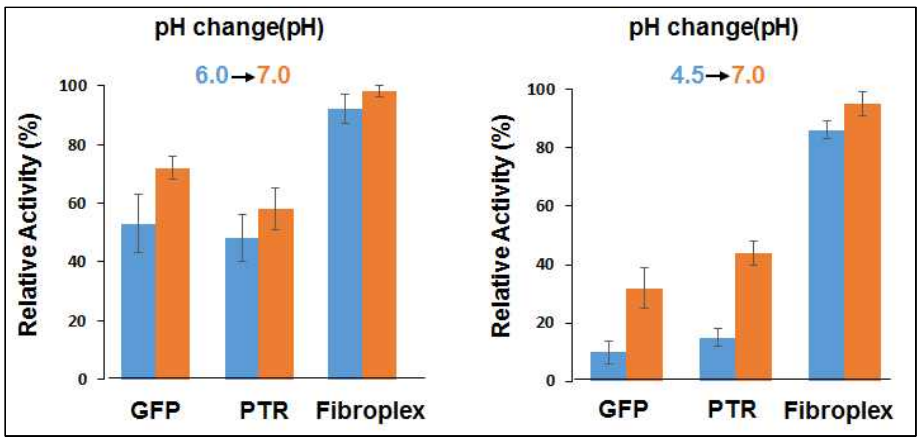

Supplementary Figure S5. The stability of GFP fluorescence

intensity at different pH levels encountered during intracellular delivery. The maximum GFP fluorescence intensity was observed at pH 7.0 in both plots. The arrows indicate an adjustment of the indicated pH to 7.0 in the same cuvette. The concentration of naive and loaded GFP proteins used was 0.1 μM, and the excitation wavelength was 460 nm.

Supplementary Figure S6. Intracellular Tyr levels were determined by immunoblot. Cells were treated with 100 nM Tyrosine-loaded fibroin particles or Fibroplex for 3 h; then, the medium was removed, and the cells were washes 3 times and incubated for an additional 72 h.

References

1. Leader, B., Q.J. Baca, and D.E. Golan, Protein therapeutics: a summary and pharmacological classification. Nat. Rev. Drug Discov., 2008. 7(1): p. 21-39.

2. Wadia, J.S., R.V. Stan, and S.F. Dowdy, Transducible TAT-HA fusogenic peptide enhances escape of TAT-fusion proteins after lipid raft macropinocytosis. Nat. Med., 2004. 10(3): p. 310-5.

3. Sun, W., et al., Self-assembled DNA nanoclews for the efficient delivery of CRISPR-Cas9 for genome editing. Angew Chem Int Ed Engl, 2015. 54(41): p. 12029-33.

4. Zuris, J.A., et al., Cationic lipid-mediated delivery of proteins enables efficient protein-based genome editing in vitro and in vivo. Nat. Biotechnol., 2015. 33(1): p. 73-80.

5. Lu, Y., W. Sun, and Z. Gu, Stimuli-responsive nanomaterials for therapeutic protein delivery. J Control Release, 2014. 194: p. 1-19.

6. Yan, M., et al., A novel intracellular protein delivery platform based on single-protein nanocapsules. Nat. Nanotechnol., 2010. 5(1): p. 48-53.

7. Cronican, J.J., et al., Potent delivery of functional proteins into Mammalian cells in vitro and in vivo using a supercharged protein. ACS Chem. Biol., 2010. 5(8): p. 747-52.

8. Heitz, F., M.C. Morris, and G. Divita, Twenty years of

cell-penetrating peptides: from molecular mechanisms to therapeutics. Br. J. Pharmacol., 2009. 157(2): p. 195-206.

9. Simeon, R.L., et al., Discovery and characterization of a new cell-penetrating protein. ACS Chem. Biol., 2013. 8(12): p. 2678-87.

10. Fagain, C.O., Understanding and increasing protein stability. Biochim. Biophys. Acta, 1995. 1252(1): p. 1-14.

11. Allen, T.M. and P.R. Cullis, Liposomal drug delivery systems: from concept to clinical applications. Adv. Drug Deliv. Rev., 2013. 65(1): p. 36-48.

12. Shete, H.K., R.H. Prabhu, and V.B. Patravale, Endosomal escape: a bottleneck in intracellular delivery. J. Nanosci. Nanotechnol., 2014. 14(1): p. 460-74.

13. Lundberg, M. and M. Johansson, Is VP22 nuclear homing an artifact? Nat. Biotechnol., 2001. 19(8): p. 713-4.

14. Martins, S., et al., Lipid-based colloidal carriers for peptide and protein delivery--liposomes versus lipid nanoparticles. Int. J. Nanomedicine, 2007. 2(4): p. 595-607.

15. Kim, S.K., M.B. Foote, and L. Huang, The targeted intracellular delivery of cytochrome C protein to tumors using lipid-apolipoprotein nanoparticles. Biomaterials, 2012. 33(15): p. 3959-66.

16. Coue, G., et al., Bioresponsive poly(amidoamine)s designed for intracellular protein delivery. Acta Biomater., 2013. 9(4): p. 6062-74.

17. Morales, D.P., et al., Targeted intracellular delivery of proteins with spatial and temporal control. Mol. Pharm., 2015. 12(2): p. 600-9.

18. Moghimi, S.M., et al., A two-stage poly(ethylenimine)-mediated cytotoxicity: implications for gene transfer/therapy. Mol. Ther., 2005. 11(6): p. 990-5.

19. Fu, J., et al., Intracellular Delivery of Functional Proteins and Native Drugs by Cell-Penetrating Poly(disulfide)s. J. Am. Chem. Soc., 2015. 137(37): p. 12153-60.

20. Altman, G.H., et al., Silk-based biomaterials. Biomaterials, 2003. 24(3): p. 401-16.

21. Saha, S., et al., Osteochondral tissue engineering in vivo: a comparative study using layered silk fibroin scaffolds from mulberry and nonmulberry silkworms. PLoS One, 2013. 8(11): p. e80004.

22. Gholipourmalekabadi, M., et al., Optimization of nanofibrous silk fibroin scaffold as a delivery system for bone marrow adherent cells: in vitro and in vivo studies. Biotechnol. Appl. Biochem., 2015. 62(6): p. 785-94.

23. Wang, Y., et al., In vivo degradation of three-dimensional silk fibroin scaffolds. Biomaterials, 2008. 29(24-25): p. 3415-28.

24. Zhao, Z., Y. Li, and M.B. Xie, Silk fibroin-based nanoparticles for drug delivery. Int. J. Mol. Sci., 2015. 16(3): p. 4880-903.

25. Pritchard, E.M. and D.L. Kaplan, Silk fibroin biomaterials for controlled release drug delivery. Expert Opin. Drug Deliv., 2011.

8(6): p. 797-811.

26. Wang, X., et al., Nanolayer biomaterial coatings of silk fibroin for controlled release. J. Control Release, 2007. 121(3): p. 190-9.

27. Wang, X., et al., Sonication-induced gelation of silk fibroin for cell encapsulation. Biomaterials, 2008. 29(8): p. 1054-64.

28. Lu, Q., et al., Green process to prepare silk fibroin/gelatin biomaterial scaffolds. Macromol. Biosci., 2010. 10(3): p. 289-98.

29. Karageorgiou, V., et al., Porous silk fibroin 3-D scaffolds for delivery of bone morphogenetic protein-2 in vitro and in vivo. J. Biomed. Mater. Res. A, 2006. 78(2): p. 324-34.

30. Shi, P., et al., Silk fibroin-based complex particles with bioactive encrustation for bone morphogenetic protein 2 delivery. Biomacromolecules, 2013. 14(12): p. 4465-74.

31. Wang, X., et al., Silk nanospheres and microspheres from silk/pva blend films for drug delivery. Biomaterials, 2010. 31(6): p. 1025-35.

32. Chang, H.I. and M.K. Yeh, Clinical development of liposome-based drugs: formulation, characterization, and therapeutic efficacy. Int. J. Nanomedicine, 2012. 7: p. 49-60.

33. Dominska, M. and D.M. Dykxhoorn, Breaking down the barriers: siRNA delivery and endosome escape. J. Cell Sci., 2010. 123(Pt 8): p. 1183-9.

34. Chan, C.L., et al., Endosomal escape and transfection efficiency of PEGylated cationic liposome-DNA complexes prepared

with an acid-labile PEG-lipid. Biomaterials, 2012. 33(19): p. 4928-35.

35. Zeng, B., H. Shi, and Y. Liu, A versatile pH-responsive platform for intracellular protein delivery using calcium phosphate nanoparticles. Journal of Materials Chemistry B, 2015. 3(47): p. 9115-9121.

36. Fujimori, F., et al., Mice lacking Pin1 develop normally, but are defective in entering cell cycle from G(0) arrest. Biochem Biophys Res Commun, 1999. 265(3): p. 658-63.

37. Hadinoto, K., A. Sundaresan, and W.S. Cheow, Lipid-polymer hybrid nanoparticles as a new generation therapeutic delivery platform: a review. Eur J Pharm Biopharm, 2013. 85(3 Pt A): p. 427-43.

38. Qin, C., et al., Tyrosinase as a multifunctional reporter gene for Photoacoustic/MRI/PET triple modality molecular imaging. Sci. Rep., 2013. 3: p. 1490.

39. Shi, H., et al., Human Serum Albumin Conjugated Nanoparticles for pH and Redox-Responsive Delivery of a Prodrug of Cisplatin. Chemistry, 2015. 21(46): p. 16547-54.

40. Zhou, C.Z., et al., Silk fibroin: structural implications of a remarkable amino acid sequence. Proteins, 2001. 44(2): p. 119-22.

41. Khositsuntiwong, N., et al., Enhancement of gene expression and melanin production of human tyrosinase gene loaded in elastic cationic niosomes. J. Pharm. Pharmacol., 2012. 64(10): p. 1376-85.

42. Greco, O., et al., Development of a novel enzyme/prodrug

combination for gene therapy of cancer: horseradish peroxidase/indole-3-acetic acid. Cancer Gene Ther., 2000. 7(11): p. 1414-20.

43. Kim, D.S., et al., Indole-3-carbinol enhances ultraviolet B-induced apoptosis by sensitizing human melanoma cells. Cell. Mol. Life Sci., 2006. 63(22): p. 2661-8.

44. Tupper, J., et al., In vivo characterization of horseradish peroxidase with indole-3-acetic acid and 5-bromoindole-3-acetic acid for gene therapy of cancer. Cancer Gene Ther., 2010. 17(6): p. 420-8.

45. Srinivasarao, M., C.V. Galliford, and P.S. Low, Principles in the design of ligand-targeted cancer therapeutics and imaging agents. Nat. Rev. Drug Discov., 2015. 14(3): p. 203-19.

46. Noble, C.O., et al., Development of ligand-targeted liposomes for cancer therapy. Expert Opin. Ther. Targets, 2004. 8(4): p. 335-53.

III. Part II

Efficiency data of intracellular recombinant protein delivery using cationic lipid coated silk fibroin particle

Woo-Jin Kim, Bong-Soo Kim, Young-Dan Cho, Won-Joon Yoon, Jeong-Hwa Baek, Kyung-Mi Woo, Hyun-Mo Ryoo*

Department of Molecular Genetics, School of Dentistry and Dental Research Institute, BK21 Program, Seoul National University, Seoul, Republic of Korea.

Keywords:
intracellular protein delivery, fibroin, cationic lipid, protein therapy

Abstract

This article presents data related to the research article "Fibroin particle-supported cationic lipid layers for highly efficient intracellular protein delivery" and focuses on the delivery efficiency aspects of the fibroin particle-cationic lipid complex (Fibroplex), including its fabrication and the intracellular delivery to the mouse skin tissue. We introduced a stable lipid-particle complex called "Fibroplex", formed by loading cargo protein onto a silk fibroin spherical particle core complexed with cationic liposomes to address the intracellular recombinant protein delivery. This system exhibits cationic charge, which is advantageous for cellular uptake. The particle core is loaded with the cargo protein with high efficiency and shows long-term release in serum environment. Fibroplex can be formed simply by mixing the particle core and cationic liposome, and this spontaneous interaction does not cause any detrimental effects on the function of cargo proteins. Lipid-particle complex structure is stable over 10 days in the serum at 37 ℃. Fibroplex was delivered at high efficiency to a wide variety of cells, including cancer cells and primary cell-lines. Also, Fibroplex loaded with two types of cargo successfully introduced them into the cytoplasm. Furthermore, Fibroplex shows successful intracellular delivery when injected with various cargo proteins such as GFP, HRP and Tyrosinase into mouse skin tissue as well as in vitro. The highlights

of this article include : (1) Data for fabrication procedure of Fibroplex, (2) loading capacity, surface charge changes of Fibroplex, and (3) Intracellular delivery aspects of Fibroin in vitro and vivo.

Specifications Table

Subject area	*Drug delivery, Biology, Material Sciences*
More specific subject area	*Biomaterial, Intracellular protein delivery, Lipid-particle complex*
Type of data	*Graph, Figure, Table*
How data was acquired	*Confocal laser Microscope, SEM, Zeta-sizer, Elisa, Western blot*
Data format	*Analyzed*
Experimental factors	*Cargo protein loading into fibroin particle*
Experimental features	*Intracellular delivery of lipid-particle complex in vitro and vivo*
Data source location	*Seoul, Republic of Korea*
Data accessibility	*Data is provided in the article*

Value of the data

- This work creates a deeper understanding of the direct recombinant protein delivery system using silk fibroin particle and lipid complex.
- The data in this article show how a design of experiment (DOE) approach can be used to produce efficient intracellular delivery of recombinant protein in various cell-lines and mouse skin model.
- The in vivo data in this article highlight the tissue uptake

efficiency and distribution of the delivered cargoes – GFP, HRP and tyrosinase protein in the mouse dorsal skin layers.

Data

Silk fibroin is a natural fibrous protein with advantages for protein loading and delivery in vitro and vivo. However, presumably because of the super-negative charge of fibroin, the application of intracellular delivery was limited. Lipid-polymer complex is formed by cationic liposomes complexed to the fibroin particle core as referenced [1]. Briefly, fibroin particles are prepared per unit weight and then dispersed by weak sonication at 10% amplitude (VC-130, Sonics, USA) for 30 seconds in 4 ℃ PBS. After particle dispersion, cationic lipids according to each weight ratio are mixed with fibroin particle solution and then vortexed for 30 seconds at room temperature. Fibroin particles and cationic lipids interact spontaneously, if incubated for 30 min at room temperature. Excess lipid is removed via light centrifugation before use (Fig. 1).

Figure 2 shows the effect of various types of fibroin particle cargo proteins on particle size and surface electrophysical characteristics. Four proteins with different sizes and characteristics GFP, HRP, Tyr(Tyrosinase) and Luc(Luciferase), respectively, showed similar size and zeta potential distributions (Fig. 1a). Fabrication of silk fibroin particle and loading cargo proteins were described previously [2]. Protein loading efficiency of fibroin

particles was measured for four representative proteins – GFP, HRP, Luciferase and tyrosinase. Proteins showed an average introduction efficiency of 50–60% (Fig. 2b). Fibroplex displayed high structural stability for a long period of time at 37°C. After Fib(GFP) containing 150 nM of GFP was formed, cells were treated with Fib(GFP) right away in one group (0 day), while other cells were treated with Fib(GFP) after it had been stored for five or 10 days at 37°C; in all cases, Fib(GFP) was taken up by the cells(Fig. 2c).

Fibroplex shows efficient intracellular delivery for various cell–lines. The same GFP protein was loaded (150nM) into fibroin particles and fibroplex, but fluorescence was not observed in cell–lines treated with anionic fibroin particles [Part (GFP)] whereas high level of fluorescence was observed in all cell–lines treated with fibroplex [Fib (GFP)] (Fig. 3a). Introduced GFP was present mainly at high concentrations around the nucleus of the cell and uniformly throughout the cytoplasm (Fig. 3b). The FACS analysis conducted on nine different cell types, including cancer and primary cells, treated with Fib(GFP) and Par(GFP) showed that only approximately 1–7% of the cells that had been treated with Par(GFP) generated fluorescence, while the Fib(GFP)–treated cells showed much higher uptake rates. Specifically, 99% of NIH3T3 and C2C12 cells were positive, and MEF, mBMSC, MDA–MB231 and PC3 cells, which are primary or cancer cell lines, showed loading rates ranging from 88 – 98%, thereby confirming that particle–lipid

complex structures can deliver EGFP into various cell types with high efficiency(Fig. 3c).

Also, Fibroplex loaded with two types of cargo successfully introduced them both into the cytoplasm. Fibroplex loaded with FITC-labeled BSA and TMR-labeled dextran penetrated the cell membrane, and different fluorescence was observed in the same cell (Fig. 4).

Fibroplex also effectively delivered HRP and luciferase into the cells. Cells treated with Fib(HRP) shows increased activity depending on treatment concentration (Fig. 5a). HRP forms active radicals that show cytotoxicity when treated with IAA(Indole-3-ace tic acid) as a substrate[3]. When 150 nM of HRP was introduced into cells via Fibroplex, they showed higher cytotoxicity with increasing concentrations of treated IAA(Fig. 5b). After the treatment with fibroplex loaded with luciferase [Fib(Luc)], the amount of intracellular enzyme was increased according to the treatment concentration similar as in the case of Fib(HRP) treatment(Fig. 5c).

To confirm whether the intracellular transport of Fibroplex occurs efficiently in vivo, we subcutaneously injected Fib(GFP) or Fib(HRP) into the dorsal skin of mice. We injected Fib(GFP) to observe the effects of transporting GFP into mouse skin cells. At 3 days after injection, we observed fluorescence in the lower layers of the dermis, and at 7 days after injection, fluorescence gradually increased in the dermis and epidermis. We did not observe such

fluorescence distributions when we injected naive GFP or Par(GFP) with the same vehicle, and no specific changes were observed in the major organs or mouse weight while the mice were being treated with Fibroplex (Fig. 6). HRP was also successfully delivered into skin tissue using Fibroplex. After injecting Fib(HRP), skin sections were assessed using dihydroethidium (DHE), a fluorogenic substrate for HRP. 7 days after injection, the skin tissues exhibited intense red fluorescence, and the distribution and enzymatic activity of HRP in skin tissue were similar to those of GFP (Fig. 6).

Fig. II-1

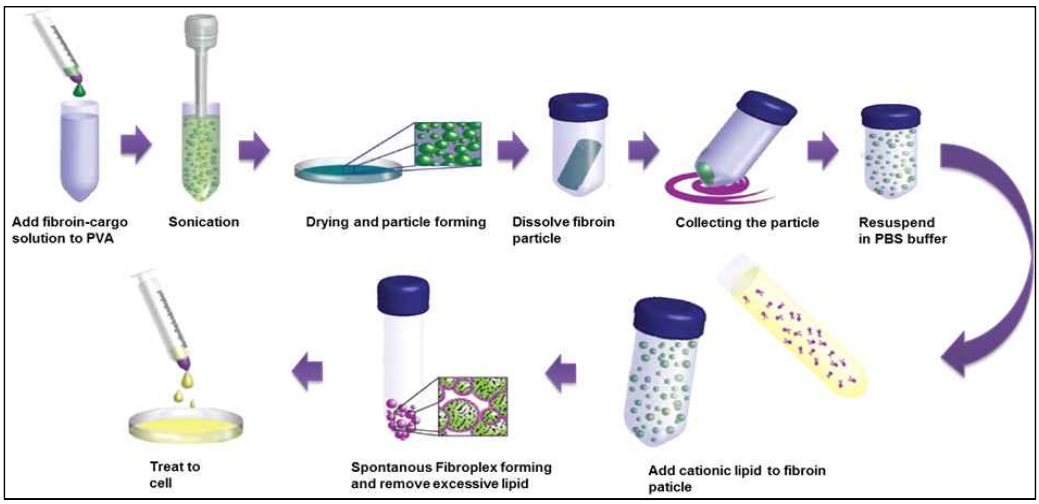

Figure II-1. Schematic illustration of fabrication of Fibroplex. PVA(poly-vinyl alcohol) was solubilized in DDW and mixed with fibroin solution for 1:4 volume ratio. Sonication was performed by 30% amplitude suggested manufacturer(VC-130, Sonics, USA) for 30 seconds at 4 ℃(for preventing heat induced damage). Cationic lipid (DOTAP:DOPE 1:1 wt%) were used for all experiments. Cationic lipids according to same weight ratio are mixed with fibroin particle and then vortexed for 30 seconds at room temperature. Fibroin particles and cationic lipids interact spontaneously, if incubated 30 min at room temperature. Excess lipid is removed via light centrifugation before treatment.

Fig. II-2

A)

	Mean size (nm)	Zeta-potential (mV)
Fibroin Particle	458.3	- 21.13 ± 2.38
GFP-loaded Particle	473.6	- 18.93 ± 3.52
HRP-loaded Particle	502.4	- 23.12 ± 5.09
Luciferase-loaded Particle	478.7	- 22.96 ± 2.47
Tyrosinase-loaded Particle	488.5	- 20.41 ± 3.76

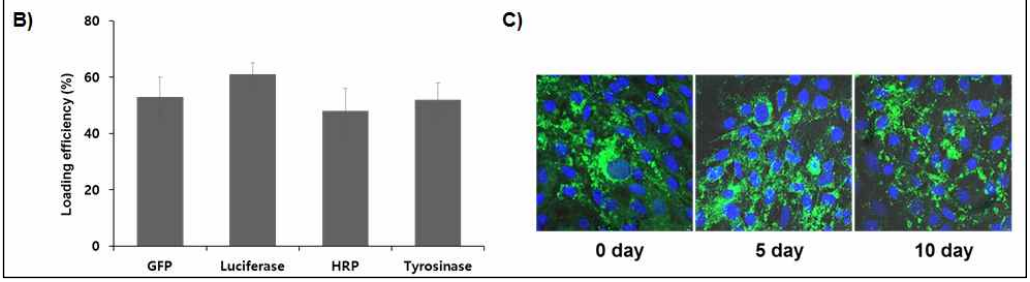

Figure II-2. Surface charge, size, loading efficiency and stability of Fibroplex.

A) fibroin solution were mixed with 150nM protein solution. Mean size and surface charge measured by zetasizer. B) The loading efficiency was measured as the amount of protein contained in the supernatant when fabricating fibroin particles by ELISA. C) Structural stability of Fibroplex was measured by intracellular delivery after incubation at 37 ° C for 10 days in serum. All error bars reflect the standard deviation of three independent biological experiments performed on different days. Scale = 5 μm.

Fig. II-3

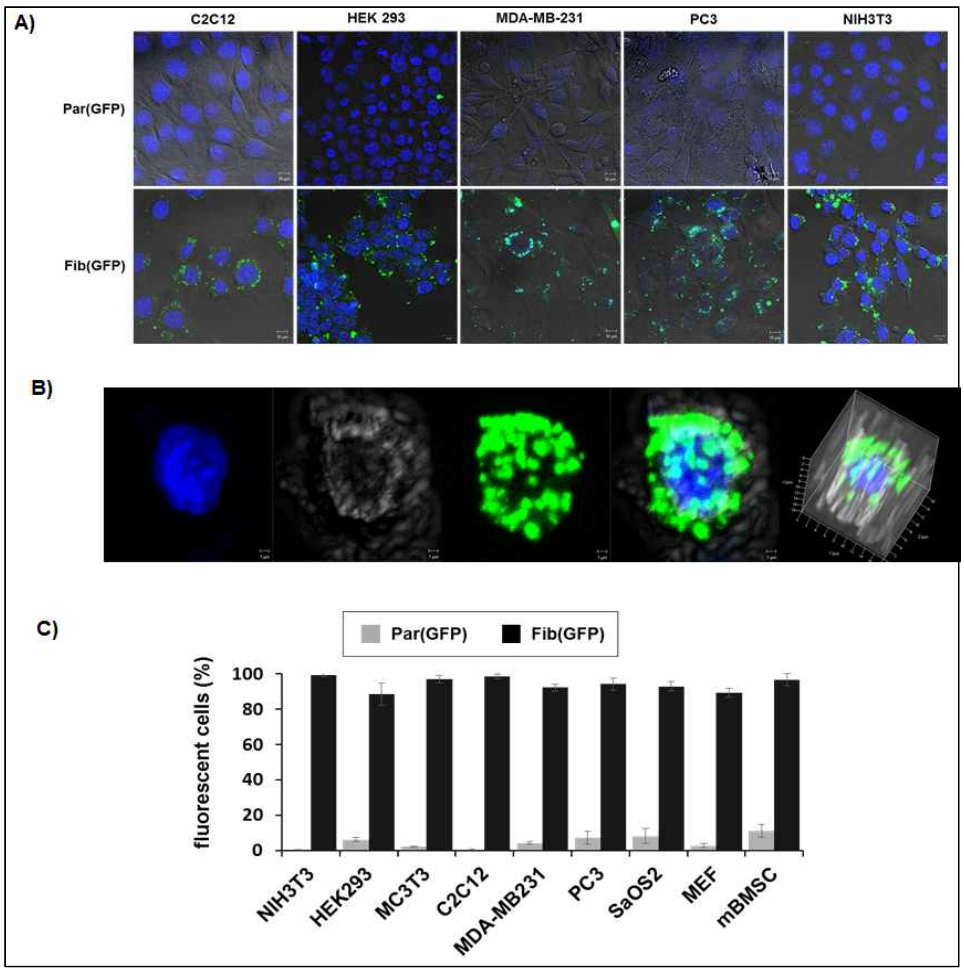

Figure II-3. In vitro Intracellular efficiency of Fibroplex. A) 5 types of cell lines - C2C12, HEK293, MDA-MB231, PC3 and NIH3T3 were treated with Fib(GFP) and Par(GFP) for 48 hours. B) Three-dimensional reconstruction of cells treated with fib(GFP) for 48 hours. C) Flow cytometric analysis were performed after treated Fib(GFP) for 48 hours. All error bars reflect the standard deviation of three independent biological experiments performed on different days. Scale = 10 μm

Fig. II-4

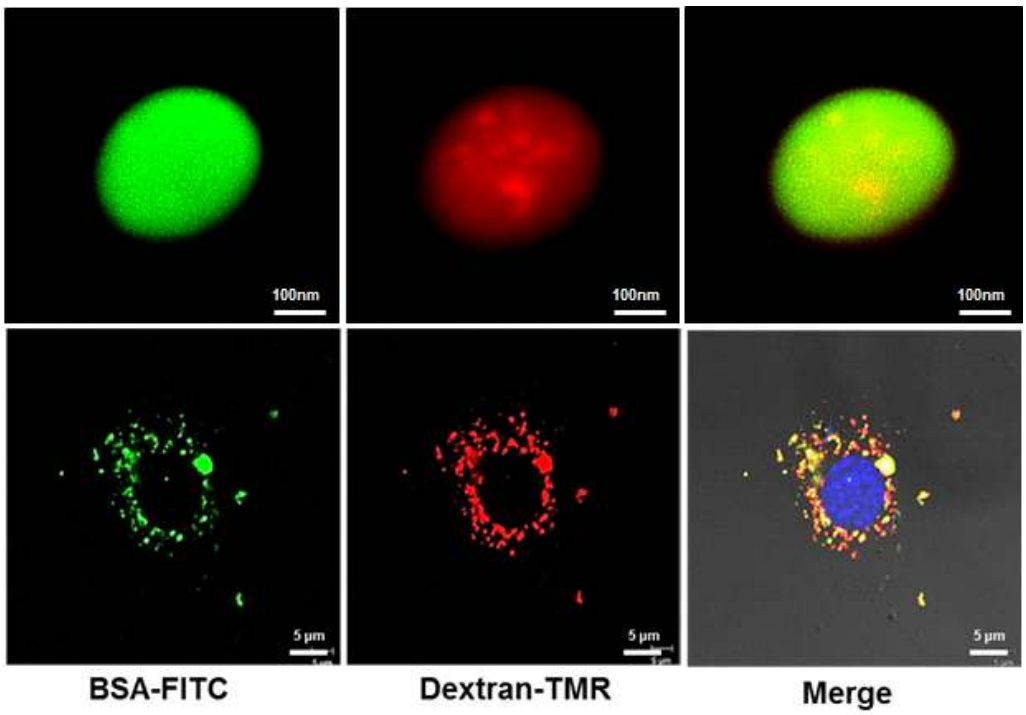

Figure II-4. Simultaneous delivery of two cargoes by Fibroplex. Two fluorescence, green and red, are observed simultaneously in one fibroin particle (Upper panel). When cells are treated, red, green, and yellow fluorescence are observed in the same cell (Lower panel).

Fig. II-5

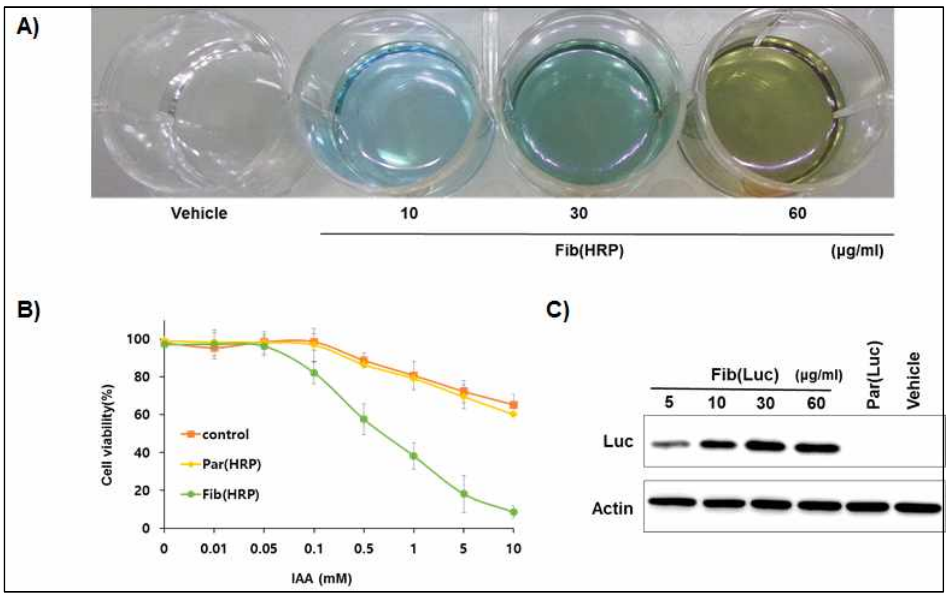

Figure II-5. Concentration-related delivery and Intracellular Enzyme Activity of uptake HRP and luciferase. A) Fib(HRP) were treated with MC3T3-E1 cells incubated 24 well plate. 10 μg of Fib(HRP) contains 34nM of HRP. After 24 hours incubation, cells were washed three times for removal of residual particles and incubated with substrate for 30 min at 37°C. B) B16-F10 cells were treated with Fib(HRP). Cytotoxicity was measured by MTT assay for each concentration. C) MC3T3-E1 cells were treated with Fib(Luc) at various concentrations, and the particles that were not internalized were removed after 48 hours and the amount of luciferase was analyzed by western blot.

Fig. II-6

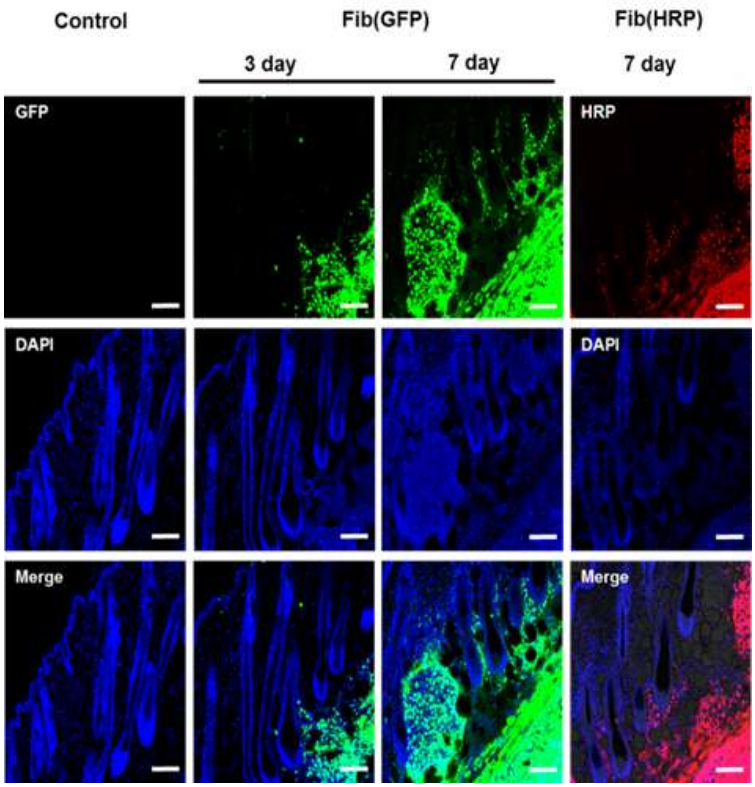

Figure II-6. In vivo delivery of Fibroplex. Fibroplex loaded with GFP or HRP were subcutaneously injected into the dorsal skin of mice. At 3 and 7 days after injection, mouse were sacrificed and frozen sections of skin tissue was analyzed by confocal laser microscopy. Scale = 50 μm

Experimental Design, Materials and Methods

2.1 Materials

All chemicals were purchased from Sigma-Aldrich unless otherwise noted and were used as received. Polyvinyl alcohol (PVA, average MW 30,000-70,000, 87-90% hydrolyzed), rhodamine B, protease XIV, horseradish peroxidase (HRP), tyrosinase (Tyr) and all other chemicals used in the study were purchased from Sigma-Aldrich (Sigma-Aldrich, USA). Enhanced green fluorescent protein (EGFP) and TAT-EGFP fusion proteins were expressed according to methods described in previous reports (Caron et al., 2001). Fusion proteins were expressed in transformed Escherichia coli BL21 and purified using a nickel-resin affinity column (Sigma-Aldrich, USA). N-[1-(2,3-Dioleoyloxy)propyl]-N,N,N-trimethylammonium methyl-sulfate (DOTAP) and 1,2-dioleoyl-sn-glycero-3-phosphoethanolamine (DOPE), and N-(7-nitrobenz-2-oxa-1,3-diazol-4-yl)dioleoyl 1,2-Dioleoyl-sn-glycero-3-phospho ethanolamine (NBD-DOPE) were purchased from Avanti Polar Lipids (Avantilipid, USA). Ultrapure water from a Milli-Q system (Millipore, USA) was used throughout this research.

2.2 Cell line cultures

The MC3T3-E1 cells were maintained in α-Minimum Essential Medium (α-MEM), and the HEK-293, NIH3T3 and C2C12 cells were maintained in Dulbecco's modified Eagle's medium (DMEM)

with 10% heat-inactivated fetal bovine serum (10% FBS) supplemented with antibiotics. Mouse embryonic fibroblasts (MEFs) were isolated from E13.5 embryos, as previously described [36]. The MEFs were grown in DMEM/10% FBS, and cells from passages 3 to 5 were used.

2.3 Preparation of fibroin particles and Fibroplex

Fabrication of fibroin particle and loading the cargoes is based on previous reports [2, 4]. Stock solutions with a concentration of 500 μM in PBS buffer, pH 7.4, were first prepared and stored at −20°C. Before loading, certain amounts of the stock solutions were added to the silk solutions to reach a drug:silk volume ratio of 1:9. After mixing, the solution was blended with the PVA solution following the steps described for the fibroin particle preparation. A 5 wt% polymer concentration and silk:PVA ratio of 1:4 was used to produce Fibroplex. Fibroplex were formed by cationic liposomes complexed to the fibroin particle core. In detail, fibroin particles are prepared per unit weight and then dispersed weakly sonicating at 10% amplitude (VC-130, Sonics, USA) for 30 seconds in 4 ℃ PBS. After particle dispersion, cationic lipids according to each weight ratio are mixed with fibroin particle solution and then vortexed for 30 seconds at room temperature. Fibroin particles and cationic lipids interact spontaneously, after incubating for 30 min at room temperature. Excess lipid is removed via light centrifugation before use. Cationic lipids (DOTAP) with 1:1 w/w PE(DOPE) were used in

all further studies and were expected to be coated on the outer surface of the fibroin particle core. As a fluorescence label for cationic lipid membranes, 0.1 wt% 7-nitrobenzofurazan-labeled DOPE(NBD-DOPE) was used to study the membrane structure of Fibroplex. Scanning electron microscopy (SEM) images were obtained with a Hitachi S-4700 field-emission instrument. Dynamic light scattering (ELSZ 1000, Photal Otsuka electronics, Japan) was used to determine the hydrodynamic size and zeta potential of Fibroplex.

2.4 In vitro cellular delivery assay

The results of cellular internalization studies were assessed via confocal laser microscopy (CLM) and fluorescence-activated cell sorting (FACS). MC3T3-E1 cells were cultured in α-MEM supplemented with 10% FBS and 1% penicillin/streptomycin. Cells (1.5×10^6 cells/100 mm plate) were seeded the day before Fibroplex was added. Fibroplex and fibroin particles loaded with equal protein concentrations were added to the cell medium. After incubation at 37°C for 12 h, the cells were washed three times with PBS containing heparin sulfate (40 μg/ml) to remove free particles. Then, the cells were incubated for an additional 24 or 48 h and either visualized with by CLM or trypsinized, centrifuged, re-suspended in PBS and analyzed via FACS. The actin staining was performed according to manufacturer's instructions. Briefly, after incubation with Fibroplex, cells were briefly washed, fixed

with 2% formaldehyde, stained with rhodamine-phalloidin for 10 min, and then observed by confocal laser microscopy (CLM).

2.5 Cell growth inhibition assay

B16-F10 melanoma cells placed in 96-well plates (3,000 cells/well) were incubated with HRP-loaded Fibroplex, fibroin particles or native HRP for 12 h; after being washed, the cells were exposed to different concentrations of IAA for 24 h. The half maximal inhibitory concentration was determined from the cell viability curve determined using MTT

2.6 In vivo evaluation of Fibroplex uptake

All animal experiments were conducted after obtaining the approval of the Seoul National University Institute of Laboratory Animal Resources and Use Committee. Each of the C57BL/6 mice (Orient Bio., Kyungi, Korea), 6-8 weeks old, was subcutaneously injected with 150 μl of a Fibroplex saline solution, a fibroin particle saline solution, or a saline solution (control). After 3 or 7 days, the mice were sacrificed, and the skin and all major organs were excised for ex vivo imaging. Then, the frozen organs were embedded in a freezing medium, and cyrosections were prepared using a microtome. The tissue sections containing Fibroplex were stained with both DAPI (for nuclei) and dihydroethidium for HRP and then observed by CLM.

References

1. Hadinoto, K., A. Sundaresan, and W.S. Cheow, Lipid-polymer hybrid nanoparticles as a new generation therapeutic delivery platform: a review. Eur J Pharm Biopharm, 2013. 85(3 Pt A): p. 427-43.

2. Wang, X., et al., Silk nanospheres and microspheres from silk/pva blend films for drug delivery. Biomaterials, 2010. 31(6): p. 1025-35.

3. Cunha, L.T., et al., Induction of oxidative stress in Prototheca zopfii by indole-3-acetic acid/HRP or 2,4-pentanedione/HRP systems and their oxidation products. Mycopathologia, 2015. 179(1-2): p. 73-9.

4. Rockwood, D.N., et al., Materials fabrication from Bombyx mori silk fibroin. Nat Protoc, 2011. 6(10): p. 1612-31.

IV. Part III Journal of Cellular Physiology. 2016 Nov 1.doi: 10.1002/jcp.25673.

Direct delivery of recombinant Pin1 protein rescued osteoblast differentiation of Pin1 deficient cells

Woo-Jin Kim, Rabia Islam, Bong-Soo Kim, Young-Dan Cho, Won-Joon Yoon, Jeong-Hwa Baek, Kyung-Mi Woo, Hyun-Mo Ryoo*

Department of Molecular Genetics, School of Dentistry and Dental Research Institute, BK21 Program, Seoul National University, Seoul, Republic of Korea.

Keywords:
Fibroin, Pin1, Nanoparticle-Lipid hybrid Complex, Protein delivery

Abstract

Pin1 is a peptidyl prolyl cis−trans isomerase that specifically binds to the phosphoserine.proline or phosphothreonine.proline motifs of several proteins. We reported that Pin1 plays a critical role in the fate determination of Smad1/5, Runx2 and β−catenin that are indispensable nuclear proteins for osteoblast differentiation. Though several chemical inhibitors has been discovered for Pin1, no activator has been reported as of yet. In this study, we directly introduced recombinant Pin1 protein successfully into the cytoplasm via fibroin nanoparticle encapsulated in cationic lipid. This nanoparticle−lipid complex delivered its cargo with a high efficiency and a low cytotoxicity. Direct delivery of Pin1 leads to increased Runx2 and Smad signaling and resulted in recovery of the osteogenic marker genes expression and the deposition of mineral in Pin1 deficient cells. These result indicated that a direct Pin1 protein delivery method could be a potential therapeutics for the osteopenic diseases.

Introduction

Under the scope of central dogma of molecular biology, the modulation of a key protein in a cell is critical for a disease treatment (Leader et al., 2008; Vaishya et al., 2015). Introduction of small chemical inhibitors or activators is one of the most popular target protein modulation methods but affects diverse nonspecific proteins and may bring unexpected adverse effects (Liu et al., 2015). Gene therapies introducing DNA or RNA also have limitations because it must go through many processes in cells for eventual protein manifestation (Imai, 2003).

Protein therapy has been considered as the safest and the most direct approach to manipulate cell function and treat human diseases (Yan et al., 2010). A majority of protein pharmaceuticals (for example, cytokines, growth factors, and monoclonal antibodies) elicit their biological activity by targeting cell surface ligands or extracellular domains. Nevertheless, advancements in molecular biology have suggested that proteins targeting intracellular biological activity could be potent therapeutics (Morris et al., 2001).

A peptidyl prolyl cis/trans isomerase (PPlase) Pin1 binds specific protein motifs and catalyzes cis/trans isomerization of the peptide bond (Yoon et al., 2013). Its association with substrates involves a WW domain that preferentially recognizes sequence motifs containing a phosphoserine or a phosphothreonine followed by a proline

(pS/pT)P motif, in target substrates(Yoon et al., 2015; Yoon et al., 2013). For this reason, Pin1 frequently functions as a binary switch flipping target substrates between two states of protein structural conformations (cis or trans), thereby leading to distinct fates of the isomerized proteins by Pin1 activity. Therefore, Pin1 is associated tightly with cell signaling and Ser/Thr kinase activity as an important structural modifier (Lee et al., 2009; Ryo et al., 2003).

We previously reported that phosphorylation (Kim et al., 2004b; Lee et al., 2003) and subsequent protein stabilization of Runx2 (Jun et al., 2010; Park et al., 2010) is required for its transactivation activity for the stimulation of osteoblast differentiation. Pin1 is a critical fate determinant for the post-phosphorylation modification of Runx2 via MAPK during osteogenic cell differentiation (Islam et al., 2016; Yoon et al., 2015; Yoon et al., 2013). Thus, modifying enzymes, including Pin1, might represent valuable drug targets to correct abnormal Runx2 activity and to ensure the optimal fate determination of osteogenic cells. Previously demonstrated results suggest that an increase Pin1 level in the osteogenic cell might promote the osteogenic differentiation.

In this study, we found that recombinant Pin1 successfully encapsulated in biocompatible natural polymer, silk fibroin, and nanoparticle and delivered to various cells including Pin1-KO mouse osteoblasts (mOB). Intracellularly delivered recombinant Pin1 protein showed a controlled release pattern and maintained its activity more than 10 days with a low toxicity. These results demonstrate that

increase of intracellular Pin1 protein level induce the stabilization of Runx2 and other osteogenic factors and consequently enhanced osteoblast differentiation.

Materials and Methods

Cell culture and reagents

Mouse embryonic fibroblast (MEF) cells were maintained in Dulbecco's modified Eagle's medium (DMEM) with 10% heat-inactivated fetal bovine serum (DMEM, 10% FBS) supplemented with antibiotics. MC3T3-E1 and primary mouse calvarial osteoblasts (mOB) were maintained in .-minimum essential medium. Mouse embryonic fibroblasts (MEFs) were isolated from E13.5 embryos of Pin Knockout (Pin1-KO) or Pin1 wild type (Pin1-WT) mice, and primary cultured cells at passages 3.5 were used for experiments. All chemicals were purchased from Sigma-Aldrich unless otherwise noted. Enhanced green fluorescent protein (EGFP) and Peptidyl-prolyl cis-trans isomerase NIMA-interacting 1 fused glutathione S-transferase (GST.Pin1) fusion proteins were purified according to methods described in previous reports (Caron et al., 2001). N-[1-(2,3-Dioleoyloxy)propyl]-N,N,N-trimethylammonium methyl-sulfate (DOTAP) and 1,2-dioleoyl-sn-glycero-3-phosphoethanolamine (DOPE) were purchased from Avanti Polar Lipids (Avantilipid, USA).

Preparations of fibroin nanoparticle encapsulated cationic lipid loaded protein (NLC).

The fibroin nanoparticle fabrication and cargo loading performed as

described previously (Wang et al., 2010). Briefly, to prepare silk fibroin aqueous stock solutions, cocoons of Bombyx mori were boiled for 30 min in an aqueous solution of 0.02 M sodium carbonate and dissolved in 9.3 LiBr solution at 60°C for 4 h. Silk and PVA stock solutions were prepared at a concentration of 5 wt%. The blended solutions were then subjected to sonication using a Vibra Ultrasonicator (VCX-130, Sonics, Newtown, CT, USA) at an energy output of 30% amplitude for 30 s on ice. For loading EGFP and GST-Pin1 into nanoparticles, the stock solutions were added to the silk solutions to reach a protein:silk volume ratio of 1:9. After mixing, the solution was blended with the PVA solution. A 5 wt% polymer concentration and silk:PVA ratio of 1:4 was used in this study. To determine protein loading in the silk spheres, the supernatants collected from the centrifugation steps were analyzed by ELISA. The amount of protein loaded onto the fibroin particles was calculated from the difference between the total amount used and the amount remaining in the supernatants. Fusing cationic lipids with silk fibroin particle cores, the proportion of cationic lipids was optimized to maintain the biocompatibility of complex. Cationic lipids (DOTAP) with 1:1 w/w PE(DOPE) were used in all further studies and were expected to be coated on the outer surface of the fibroin nanoparticle core.

Mouse strains

Pin1-KO mice have been described previously (Islam et al.,

2014). All animal studies were reviewed and approved by the Special Committee on Animal Welfare (SNU-140228-1-4), Seoul National University, Seoul, Republic of Korea. Male mice were used for all experiments.

Drug release from fibroin nanoparticle encapsulated cationic lipid loaded protein (NLC)

NLC loaded with the GFP or Pin1 was suspended in 1 ml of PBS buffer, pH 7.4. The samples were incubated at 37°C under slow shaking. At certain time points, samples were centrifuged at 16,000 rpm for 10 min with a microcentrifuge (5417R,Eppendorf,Germany), the supernatants were carefully transferred to empty tubes, and the pellets were suspended in 1 ml of PBS buffer to continue the release study. The absorbance of the collected supernatants was then measured at 555 nm. The amount of model drug was then calculated based on a standard curve. The cumulative release was obtained by comparing the data with the original extent of sphere loading. For each model drug, at least three samples were prepared to obtain statistical data.

In vitro cellular delivery assay

The results of cellular internalization studies were assessed via confocal laser microscopy (CLM) and fluorescence-activated cell sorting (FACS). Cells (1.5 X 10^6 cells/100 mm plate) were seeded the day before treatment. NLC, fibroin nanoparticles loaded with

equal protein concentrations or naive protein were added to the cell medium. After incubation at 37°C for 24 h, the cells were washed three times with PBS containing heparin sulfate (40 μg/ml) to remove free particles. Then, the cells were incubated for an additional 24 or 48 h and either visualized with by CLM or trypsinized, centrifuged, re-suspended in PBS and analyzed via FACS. The actin staining was performed according to manufacturer's instructions. Briefly, after incubation with the NLCs, cells were briefly washed, fixed with 2% formaldehyde, stained with rhodamine-phalloidin for 10 min, and then observed by CLM.

Cytotoxicity assay

The toxicity of the NLC was assessed by the MTT assay. MC3T3-E1 cells (7,000 cells/well) were seeded on a 96-well plate the day prior to NLC exposure. Different concentrations of NLC were incubated with the cells for 24 h; subsequently, the cells were incubated with fresh media for different times. Cationic lipids (1:1 wt% DOTAP:DOPE) and fibroin nanoparticles were treated as controls. Untreated cells were used as the 100% cell proliferation control.

RNA extraction and quantitative real-time PCR (qPCR) expression analyses

Total RNA was extracted from the whole tibia of newborn mice (crushed in liquid nitrogen and homogenized) or cultured cell using

the easy-BLUE, total RNA extraction kit. cDNAs were synthesized from 1mg of total RNA using the SuperScript II first-strand synthesis system Reverse Transcriptase kit (Invitrogen). Approximately 100 ng of RNA was used for each reaction in relative qPCR.

Alkaline phosphatase (ALP) staining

For ALP staining, cells were washed twice with phosphate-buffered saline, fixed with 2% paraformaldehyde, and stained for ALP-induced chromophores according to the manufacturer's instructions (Sigma-Aldrich).

Alizarin red S staining

Cells were washed with Ca^{2+}-free PBS for three times and fixed in 1% formaldehyde/PBS for 20 min at 4°C. After five washes with distilled water, the cells were stained in 1% alizarin red S solution for 5 min to visualize matrix calcium deposition.

Results

Preparations of GFP and Pin1 loaded fibroin nanoparticle supported cationic lipid layer

Pioneered by Wang et al., a new aqueous-based preparation method for silk spheres for encapsulating wide range of molecular hydrophobicity and charges like recombinant protein was developed (Wang et al., 2010). The preparation was based on phase separation between silk fibroin and polyvinyl alcohol (PVA) within water soluble condition. However, the nanoparticles made of fibroin protein maintained their highly anionic character.

To overcome this negative surface charge for penetrating cellular membrane, we encapsulate nanoparticle with cationic lipid layers (DOTA-DOPE 1:1 weight ratio). As schematic illustration in Fig 1A shows, the negative charge of fibroin nanoparticle increased to 17.3 ± 3.42 mV when they form nanoparticle - cationic lipid complex. Positive charged complex was successfully incorporated cell membrane and uptake intracellular space, slowly degraded and released its cargo.

The shape of the complex is comprised of a thin lipid layer that strongly interact with the fibroin nanoparticle surface. We observed that the shape of spherical fibroin nanoparticle was maintained even after the cargo protein was loaded (Fig. 1B, right). And, formation of the resultant complex was sobserved with NBD labeled cationic

lipids and Rhodamin B labeled fibroin particles. Observations under a confocal laser microscop (CLM) showed a green ring-like coated layer surrounding the red particle core. Moreover, the image of 3D reconstruction by Z axis section also confirmed the structure of lipids layers encapsulating the fibroin nanoparticles (Fig. 1B, left).

This fibroin particle-cationic lipid complex (NLC) showing high protein loading capacities around (GFP was 63 % and Pin1 was 67 %, respectively). The protein loaded nanoparticle size was around 470 ± 228 nm, surface charge was -21.13 ± 4.78 mV as analyzed by zetasizer (Fig. 1C and 1D).

Delivery of recombinant GFP and Pin1 protein into cells

Before confirming the osteogenic effect of delivered recombinant Pin1, we tested whether the NLC could mediate intracellular delivery of model protein GFP. MEF cells were treated with NLC loading GFP [NLC(GFP)]. FACS analysis revealed that 97% of the cells incubated with NLC (GFP) were positive, showing a relatively higher transduction efficiency than naive GFP (GFP) or GFP-loaded particles [Par(GFP)], 2 % and 5.3 %, respectively (Fig. 2A) When the cells were observed with CLM, cells that had been treated with GFP or Par (GFP) showed no or low fluorescence, while most of the cells that had been treated with NLC (GFP) yielded a strong fluorescence (Fig. 2B).

Recombinant Pin1 was encapsulated successfully into fibroin particles. Also, as shown in Fig. 2C, WT mOB cells treated with

NLC (Pin1) showed high Pin1 level in the cytoplasm. After 24 hr, delivered Pin1 protein was detected with anti-GST antibody (Red). Moreover, when Pin1-KO mOB were treated with NLC(Pin1), the concentration of Pin1 in cells increased in proportion to the amount of NLC(Pin1)

Delivered recombinant Pin1 maintained enzymatic activity with low cyto-toxicity

Delivered Pin1 protein maintained its enzymatic function. Mouse embryonic fibroblast(MEF) showed defect in G1/S transition and slower growth, expression of Pin1 promote cell-cycle progression from G1 into the S phase. Pin1-KO MEFs were treated with naive Pin1 or Par (Pin1), no enzymatic activity could be detected; in contrast, when cells were treated with NLC(Pin1) for 4 days and analyzed by flow cytometry stained with propidium iodine(PI), they showed an increase ratio of the cells in the S phase as expected, and the ratio was directly proportional to the concentration (Fig. 3A).

Uptake of nanoparticles by cells has low influence on cell viability. The viability of MEF cells after 48 h of incubation with the fibroin nanoparticles, free cargo protein, as well as the NLC was evaluated by MTT assays. A similar level of cell viability was confirmed that showed under 3 % decrease of cell viability after 24 h of exposure to NLC and under 4 % after 72 h of exposure. The fibroin nanoparticles in the same concentrations as their noncomplexed free

components exhibited similar toxicity. Also, the types of loading cargo not effect to cytotoxicity (Fig. 3B)

Long-term protein release properties *in-vitro* and *vivo*

The cargo release profiles of NLC turned out to be a compromise between the nanoparticle-cargo interaction and the molecular weight. Following a short and low-level (about 1%) initial burst release, the fluorescein isothiocyanate (FITC) and rhodamine B (RhB) were released slowly, with less than 14 % of the total load being released within 10 weeks (Fig. 4A). In contrast, TMR-BSA, GFP and Pin1 were released much faster, with more than 47 % - respectively, 54 %, 47 % and 51 % of total load being released within 4 weeks at a nearly zero-order release rate (Fig. 4A).

Stable sustained release profile of NLC for protein drugs also resulted in a long-term protein activity inside the cells. We treated NLC(GFP) and NLC(Pin1) to the cells and observed the cells for 10 days; the maximum GFP activity was observed in 4-5 days, and the fluorescence maintained continuously until after 10 days. Also, the same release observed by anti-GST immunoblot when Pin1 was delivered into the cells (Fig. 4B)

Pin1-KO MOBs Induced osteogenic faith by recombinant Pin1 delivery

Our previous reports demonstrated that Pin1-KO mice showed mineralization deficient phenotypes (Yoon et al., 2013), which

suggested that Pin1 is involved in the regulation of canonical BMP signaling by maintaining phosphorylation of Smad1/5 and stabilization of Runx2 level (Yoon et al., 2014; Yoon et al., 2015; Yoon et al., 2013).

Delivery of recombinant Pin1 recovered the osteogenic induction of Pin1−KO cells to the same level as Pin1 WT. The mRNA levels of four typical bone markers and Runx2 target genes, Col1A1, alkaline phosphatase (Alp), osteocalcin (Oc), and the osteogenic transcription factor Dlx5 and Runx2, were dramatically reduced in the Pin1−KO mouse calvarial osteoblasts. However, in cells treated with NLC (Pin1) for 48 h, the four genes mRNA level was recovered about 80 − 90% of that seem in WT (Fig. 5A) The effect of delivered Pin1 on Alp protein activity during osteogenic media stimulation, showed strongly recovery in Pin1−KO MOBs. Under Alp staining assay, Pin1−KO MOB showed no staining, however, the cells treated with NLC(Pin1) for 3 days showed similar Alp activity with that of WT cells (Fig. 5B). The alizarin red S staining of Pin1−KO MOBs also indicated that mineral deposition potential was recovered in cells treated with NLC(Pin1) (Fig. 5C).

Introduced recombinant Pin1 enhanced SMAD and Runx2 stability

Our previous report demonstrated that interaction between Runx2 and Pin1 regulate Runx2 stability by increasing its phosphorylation via ERK/MAPK and decreasing the ubiquitination (Yoon et al., 2014; Yoon et al., 2015). Also, Pin1 and SMAD1/5 interaction induced

SMAD stabilization through the suppression of the Smad1.Smurf1 interaction. Moreover, BMP2-induced osteoblast differentiation is more strongly promoted by overexpression of only Pin1(Yoon et al., 2015).

Osteogenic stimulation showed immediate early phosphorylation of ERK in both MOBs from the Pin1-KO or WT mice (Fig. 5D). As observed in previous literature, although high phosphorylated ERK, endogenous Runx2 protein levels were strongly down-regulated by Pin1 deficiency. However, the Runx2 protein level was recovered by treatment with NLC(Pin1) for 3 days but was still decreased in Pin1 loaded fibroin nanoparticle[Par(Pin1)] treated group (Fig. 5D).

Smad1 and Smad5 (Smad1/5) and phosphorylated Smad1/5 (ρ-Smad1/5) are remarkably reduced in Pin1 deficient cells. Introduction of Pin1 via NLC(Pin1) significantly restored both Smad1/5 expression and phosphorylation level (Fig. 5E).

Discussion

Following the identification of BMPs and their signaling path there have been important discoveries and clinical reports on their use for bone regeneration (Ryoo et al., 2006). We reported that phosphorylation of the Smad1 linker region accelerates its interaction with Smurf1, an E3 ligase of Smad1, followed by proteolytic degradation (Aragon et al., 2011), However, it appears that proteolytic consequences are dependent on the conformational status of Smad1 protein because Pin1 is sufficient to prevent the Smurf1.Smad1 interaction as well as Smad1 ubiquitination (Yoon et al., 2014).

MAPK or FGF2 signaling is also very important for bone mineralization (Ge et al., 2009; Hurley et al., 1996; Kim et al., 2004a). FGF-2 and BMP-2 have a synergistic effect on fracture healing; FGF-2 has a critical function at the early stage while BMP-2 promotes mineralization at the later stage (Agas et al., 2013; Nakamura et al., 2005; Yoon et al., 2014). We also reported that FGF2-induced phosphorylation and subsequent acetylation and can stimulate Runx2 transactivation activity (Park et al., 2010). FGFR2 activation, secondary to ligand binding, leads to MEK1/2 activation, which subsequently stimulates Runx2 transactivation activity. Pin1-dependent isomerization is a critical intermediate step between the phosphorylation and the acetylation of Runx2, thereby

enhancing the functional activity of Runx2 (Jeon et al., 2006; Park et al., 2010).

Until now, it has been widely accepted that Pin1 is a molecular switch to determine the fate of numerous phosphoproteins, especially regarding the regulation of protein stabilization (Liou et al., 2011; Mantovani et al., 2007). In addition, Pin1 has been shown to function in key roles in both BMPs and FGF signaling regulation for formation of new bones (Huang et al., 2013; Shen et al., 2013; Yoon et al., 2014; Yoon et al., 2015). Thus, increasing the level of Pin1 in the cell might be a potentially valuable protein drug for ensureing the optimal fate determination of osteogenic cells specifically. Our results suggested that a gene deficieny could be recovered functionally by direct delivery of the deficient recombinant protein to the cell (Fig. 1). Delivery of functional active proteins would mimic gain of function such as we observed with cells that had a physiological defect like cell cycle arrest and recovered high proliferation capacity after the deficeit protein was directly delivered inside the cells (Fig. 1). However, direct delivery of recombinant protein is still hampered by many obstacles and its delivering scaffold is also important.

Recently, integrated systems known as lipid.polymer hybrid nanoparticles have been introduced in an effort to mitigate some limitations associated with liposomes and nanoparticles (Mandal et al., 2013; Raemdonck et al., 2014). The biomimetic characteristics of lipids and architectural advantage of polymer core are combined

to yield a theoretically superior delivery system (Hasan et al., 2012; Jain et al., 2013).

Silk fibroin is a natural fibrous protein with a unique structure of repeating hydrophobic and hydrophilic domains that has many advantages, such as in vivo biodegradation (Wang et al., 2008a); this protein has been extensively studied for in vivo applications(Chung et al., 2014; Wang et al., 2008b; Yan et al., 2013). In particular, fibroin has unique advantages for protein delivery, including a high loading capacity, controllable drug release kinetics, and the ability to encapsulate cargo proteins without covalent bonds or the use of organic solvents during fabrication, which could disrupt the activity of the cargo proteins (Wang et al., 2010). Previous studies have reported the successful in vivo application of a silk fibroin scaffold for protein drugs but it was not for intracellular delivery, presumably because of the super-negative charge of fibroin particles, which inhibits cellular uptake.

Cationic lipid formulations have enabled transfection with DNA or RNA to become routine techniques in basic research and have even been used in clinical trials (Felgner and Ringold, 1989; Malone et al., 1989). Notably, the fusion of liposomes with the endosomal membrane during endosome maturation can enable the efficient endosomal escape of cationic lipid-delivered cargo (Chan et al., 2012; Yasuda et al., 2005). Because proteins, in contrast to nucleic acids, are chemically diverse with no dominant electrostatic property, no lipid formulation is likely to drive the efficient delivery

of all proteins into mammalian cells. However, while proteins can be complexed nonspecifically and delivered by rehydrated lipids in vitro, protein complexation is dependent on high protein concentrations, and is generally inefficient, and has not been widely adopted (Yan et al., 2010). Specialty commercial reagents developed for protein delivery have shown modest and variable efficiency with different protein cargos (Yang et al., 2015).

Our results show that fibroin nanoparticle supported lipid complex can be fabricated with natural silk fibroin protein and clinically applicable cationic lipids to achieve high intracellular delivery efficiency with enhanced capacity and stability (Fig. 2 and 3). Also these proteins can be loaded into the nanoparticles without additional covalent bonds, this was critical for maintained cargo protein activity (Altinoglu et al., 2016).

the NLC showed supreme biocompatibility and high loading capacities of protein cargos, enabling the stable, long-term, intracellular release and activity in the cytoplasm (Fig. 1 and 3). In biocompatibility, the hyper-anionic charge of fibroin nanoparticles caused by particle-lipid complexation can be used to control transfection efficiency and reduce unexpected cationic lipid toxicity due to over treatment. In fact, cationic delivery systems are often toxic when delivered in high concentrations; however, when we performed an MTT assay, even high concentrations of the NLC showed low cytotoxicity (Fig. 3B). And, the NLCs shows a stable sustained release profile in vitro. We investigated the cumulative

release patterns of fibroin nanoparticles and NLCs, and found that approximately 60% release of loaded protein occurred over 100 days, following a short and low-level (about 1%) initial burst release, probably due to the release of residual drug that remained on or near the surface of fibroin nanoparticles; in contrast, the maximum release of fluorescein isothiocyanate(FITC) and rhodamine B, which are relatively small and hydrophobic molecules, was 11% over the same period. Therefore, NLC showed an effective and selective release profile for proteins (Fig. 3D). The stable, sustained release profile of NLCs for protein drugs also resulted in long-term intracellular protein activity (Fig. 4B). Compare of DNA transfection with NLC, the maximum expression of transfected gene was 24~72 hours, direct delivery of recombinant protein with slow release in cytoplasm is quit applicable for long-term treatments required in conditions such as hereditary disease or tissue regeneration.

The Pin knock-out newborn mice showed a range of CCD phenotypes such as abnormal development of the cranial bones and clavicle with delayed ossifications and hypomineralization of the whole skeleton (Yoon et al., 2013). Genetically, CCD results from the haploinsufficiency of RUNX2, and Pin1 plays a critical role in the Runx2 protein stabilization (Callea et al., 2012). Also, the levels of Smad1 protein expression were remarkably suppressed in the adult bone marrow of Pin1-deficient mice, demonstrating attenuated canonical BMP2 signaling. In addition, BMP2-induced osteoblast

differentiation is more strongly promoted by overexpression of only Pin1 (Yoon et al., 2013). These previous reports demonstrated that prolyl isomerization of phospho-Smad and Runx2 by Pin1 is of great importance for adult bone mineralization.

Direct delivery of recombinant Pin1 successfully promote long-term Runx2 stability and phosphorylation of Smad1/5 (Fig. 5D and 5E). These results, consequently related with the interactions of the delivered recombinant Pin1 with phosphorylated Runx2 induce its conformation change promote Runx2 stabilization. Also, the delivered Pin1 probably prevent Smad1 linker region interaction with Smurf1, an E3 ligase of Smad1 leading to the increase of long-term p-Smad level (Yoon et al., 2014). Up-regulating these two main osteogenic signals resulted in recovery of the osteogenic marker genes expression (Fig. 5A and 5B) and in-vitro mineral deposition (Fig. 5C).

In conclusion, our data demonstrate that direct delivery of recombinant Pin1 via fibroin nanoparticle encapsulated cationic lipid complex successfully maintain functional interaction with Runx2 or Smad1/5 and enhances canonical BMP2 signaling and is crucial for BMP2-induced osteogenic differentiation. Therefore, we suggest here that direct delivery of modifying enzymes, such as Pin1, might represent valuable protein drug to correct abnormal Runx2 activity and to ensure the optimal fate determination of osteogenic cells in the differentiation and development of bone.

Figure III-1

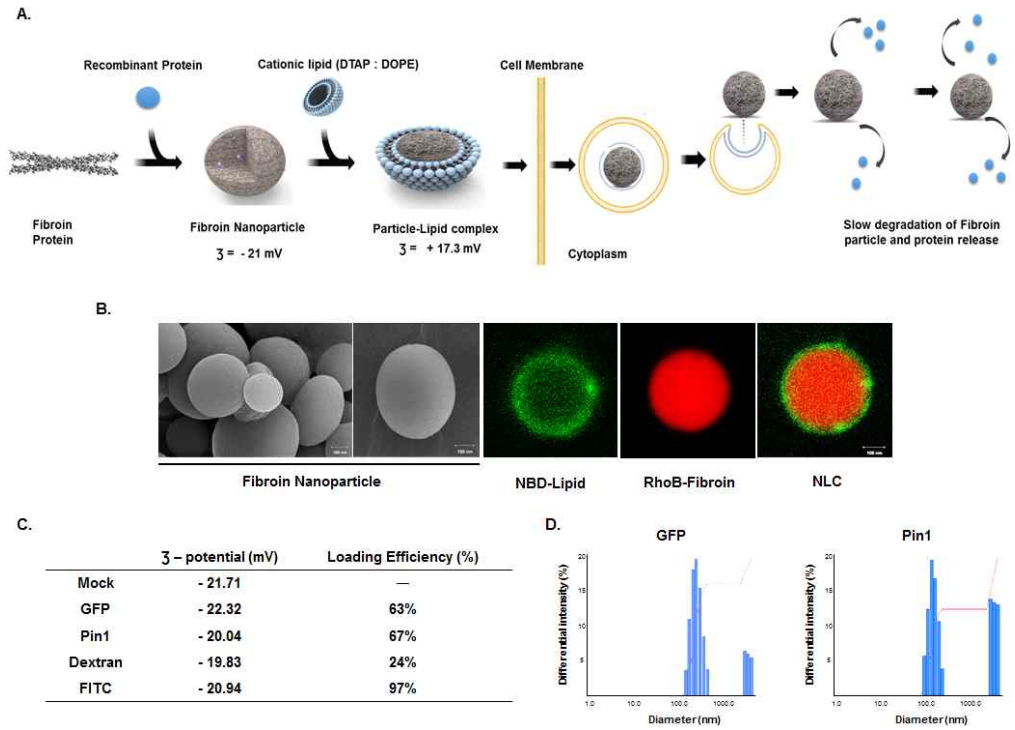

Figure III-1. Characterization of nanoparticle-lipid complex for direct protein delivery.

(A) Schematic illustration of fibroin nanoparticle-cationic lipid complex formation and cytosolic delivery process (B) Scanning electron microscopic images of Pin1 loaded fibroin nanoparticles [Par(Pin1)] (Left) and fibroin nanoparticles were labled with rhodamine B (RhB, Red) and supported by NBD-labeled cationic liposomes (Green) revealed nanoparticle core encapsulated lipid envelope. Scale bars represent 100 nm. (C) Surface charges and loading efficiency in various cargo types analyzed by zetasizer (Otsuka, Japan). (D) Average sphere hydrodynamic diameters and polydispersities obtained using zetasizer.

Figure III-2

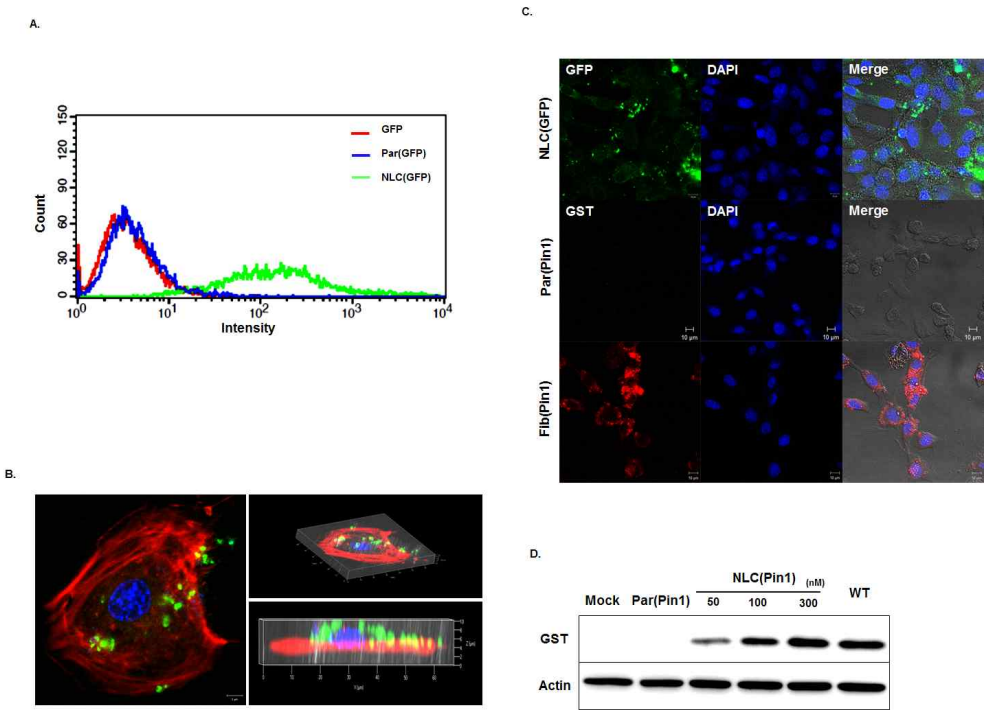

Figure III-2. Nanoparticle . lipid complex delivered recombinant GFP and Pin1 proteins into the cytoplasm with high efficiency.

(A) Flowcytometric analysis (FACs, BD Biosciences, USA) of MEF cells incubated with 150 nM GFP for 48 h via different delivery systems, i.e., naive GFP (GFP), GFP loaded fibroin nanoparticle [Par(GFP)] or nanoparticle-lipid complex [NLC(GFP)]. (B) Confocal laser microscopy (CLM) images showing the delivery of GFP via NLC. MEF cells were treated with NLC(GFP) loaded with 150 nM GFP. Cells were visualized with DAPI (for nuclei) after 48 h of treatment. Cells were counter-stained with rhodamine-phalloidin (for F-actin) to identify the cell boundaries. All scale bars represent 10 μm. (C) Intracellular uptake of GFP and

Pin1 analyzed by CLM. GST fused Pin1 (GST-Pin1) detected with anti GST antibody (Red). (D) GST-Pin1 protein uptake was observed in MEF cells that were treated with different concentrations shown in the figure. The cell lysates were subjected to Western blot followed by immunoblotting with GST antibody.

Figure III-3

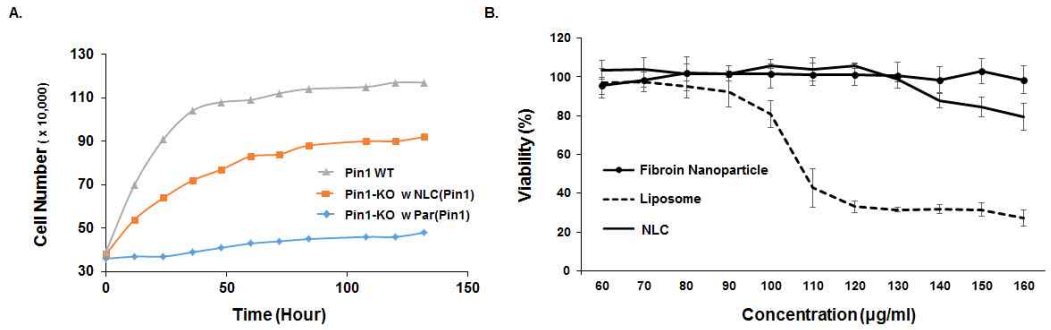

Figure III-3. Enzymatic function recovery of Pin1 in Pin1-KO cells with low cytotoxicity.

(A) Pin1-KO MEFs at 30% confluency were cultured for 6 days. The number of cells were counted at the indicated time points. (B) MTT assay results showing cell viability after treatment with different concentrations of Fibroin nanoparticle, cationic liposome (DOTAP:DOPE) and NLC for 48 h.

Figure III-4

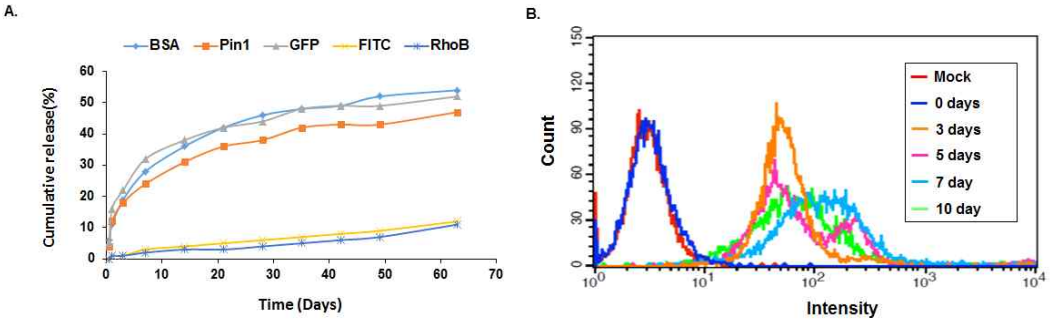

Figure III-4. Long-term stable cargo release of nanoparticle-lipid complex

(A) Cumulative release of NLCs loaded with various model drugs showing stable release profiles for hydrophilic macromolecules, i.e., proteins, as determined by measuring the amount of drug present in the supernatant fraction after centrifugation. (B) Flowcytometry analysis of cells for 10 days of treatment with NLC(GFP).

Figure III-5

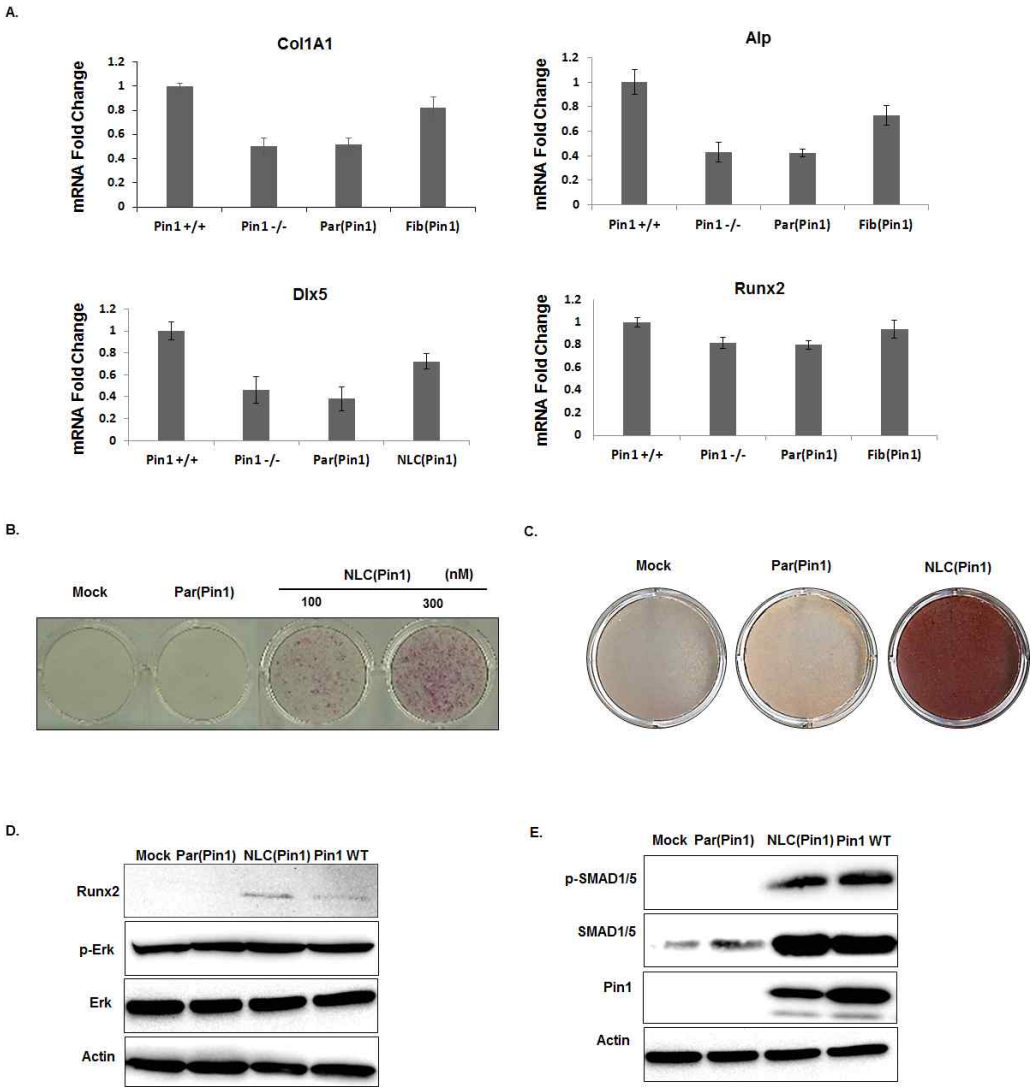

Figure III-5. Direct recombinant Pin1 delivery mediate osteogenic differentiation.

(A) Quantitative RT-PCR analyses of bone marker genes in RNA extracted from Pin1-KO and Pin1-WT mOB. mRNA expression was

observed for ColA1 (α1(1)collagen), Alp(alkaline phosphatase), Oc (Osteocalcin), Dlx5, and Runx2. (B) Confluent cells were cultured with or without a 24 h pretreatment of NLC(Pin1) or Par(Pin1) (loading 150nM of Pin1), followed by culturing for 5 days and Alp staining using a commercial kit (C) Osteoblast cells isolated from 18.5 days of Pin1-KO and Pin1-WT mice were cultured in osteogenic medium for 21 days and analyzed by alizarin red staining. (D) determination of Runx2 and Erk protein levels depending on the Pin1 treatment via NLC(Pin1) or Par(Pin1) in mOBs. (E) Prolonged maintained phosphorylation SMAD1/5 protein was observed in Pin1-KO and Pin1-WT mOB cells that were cultured for 36 h. The cell lysates were subjected to Western blot followed by immunoblotting with Smad 1/5 antibody and Smad1/5-TP antibody (recognizing the phospho-Smad tail).

References

Agas D, Sabbieti MG, Marchetti L, Xiao L, Hurley MM. 2013. FGF-2 enhances Runx-2/Smads nuclear localization in BMP-2 canonical signaling in osteoblasts. J Cell Physiol 228(11):2149-2158.

Altinoglu SA, Wang M, Li KQ, Li Y, Xu Q. 2016. Intracellular delivery of the PTEN protein using cationic lipidoids for cancer therapy. Biomater Sci.

Aragon E, Goerner N, Zaromytidou AI, Xi Q, Escobedo A, Massague J, Macias MJ. 2011. A Smad action turnover switch operated by WW domain readers of a phosphoserine code. Genes Dev 25(12):1275-1288.

Callea M, Fattori F, Yavuz I, Bertini E. 2012. A new phenotypic variant in cleidocranial dysplasia (CCD) associated with mutation c.391C>T of the RUNX2 gene. BMJ Case Rep 2012.

Chan CL, Majzoub RN, Shirazi RS, Ewert KK, Chen YJ, Liang KS, Safinya CR. 2012. Endosomal escape and transfection efficiency of PEGylated cationic liposome-DNA complexes prepared with an acid-labile PEG-lipid. Biomaterials 33(19):4928-4935.

Chung YG, Algarrahi K, Franck D, Tu DD, Adam RM, Kaplan DL, Estrada CR, Jr., Mauney JR. 2014. The use of bi-layer silk fibroin scaffolds and small intestinal submucosa matrices to support bladder tissue regeneration in a rat model of spinal cord injury. Biomaterials

35(26):7452-7459.

Felgner PL, Ringold GM. 1989. Cationic liposome-mediated transfection. Nature 337(6205):387-388.

Ge C, Xiao G, Jiang D, Yang Q, Hatch NE, Roca H, Franceschi RT. 2009. Identification and functional characterization of ERK/MAPK phosphorylation sites in the Runx2 transcription factor. J Biol Chem 284(47):32533-32543.

Hasan W, Chu K, Gullapalli A, Dunn SS, Enlow EM, Luft JC, Tian S, Napier ME, Pohlhaus PD, Rolland JP, DeSimone JM. 2012. Delivery of multiple siRNAs using lipid-coated PLGA nanoparticles for treatment of prostate cancer. Nano Lett 12(1):287-292.

Huang GL, Qiu JH, Li BB, Wu JJ, Lu Y, Liu XY, He Z. 2013. Prolyl isomerase Pin1 regulated signaling pathway revealed by Pin1 +/+ and Pin1 -/- mouse embryonic fibroblast cells. Pathol Oncol Res 19(4):667-675.

Hurley MM, Marcello K, Abreu C, Kessler M. 1996. Signal transduction by basic fibroblast growth factor in rat osteoblastic Py1a cells. J Bone Miner Res 11(9):1256-1263.

Imai E. 2003. Gene therapy for renal diseases: its potential and limitation. J Am Soc Nephrol 14(4):1102-1104.

Islam R, Bae HS, Yoon WJ, Woo KM, Baek JH, Kim HH, Uchida T, Ryoo HM. 2014. Pin1 regulates osteoclast fusion through suppression of the master regulator of cell fusion DC-STAMP. J Cell Physiol 229(12):2166-2174.

Islam R, Yoon WJ, Ryoo HM. 2016. Pin1, the Master Orchestrator

of Bone Cell Differentiation. J Cell Physiol.

Jain S, Kumar S, Agrawal AK, Thanki K, Banerjee UC. 2013. Enhanced transfection efficiency and reduced cytotoxicity of novel lipid-polymer hybrid nanoplexes. Mol Pharm 10(6):2416-2425.

Jeon EJ, Lee KY, Choi NS, Lee MH, Kim HN, Jin YH, Ryoo HM, Choi JY, Yoshida M, Nishino N, Oh BC, Lee KS, Lee YH, Bae SC. 2006. Bone morphogenetic protein-2 stimulates Runx2 acetylation. J Biol Chem 281(24):16502-16511.

Jun JH, Yoon WJ, Seo SB, Woo KM, Kim GS, Ryoo HM, Baek JH. 2010. BMP2-activated Erk/MAP kinase stabilizes Runx2 by increasing p300 levels and histone acetyltransferase activity. J Biol Chem 285(47):36410-36419.

Kim HJ, Park HD, Kim JH, Cho JY, Choi JY, Kim JK, Kim HJ, Shin HI, Ryoo HM. 2004a. Establishment and characterization of a stable cell line to evaluate cellular Runx2 activity. J Cell Biochem 91(6):1239-1247.

Kim YJ, Lee MH, Wozney JM, Cho JY, Ryoo HM. 2004b. Bone morphogenetic protein-2-induced alkaline phosphatase expression is stimulated by Dlx5 and repressed by Msx2. J Biol Chem 279(49):50773-50780.

Leader B, Baca QJ, Golan DE. 2008. Protein therapeutics: a summary and pharmacological classification. Nat Rev Drug Discov 7(1):21-39.

Lee MH, Kim YJ, Kim HJ, Park HD, Kang AR, Kyung HM, Sung JH, Wozney JM, Kim HJ, Ryoo HM. 2003. BMP-2-induced Runx2

expression is mediated by Dlx5, and TGF-beta 1 opposes the BMP-2-induced osteoblast differentiation by suppression of Dlx5 expression. J Biol Chem 278(36):34387-34394.

Lee TH, Tun-Kyi A, Shi R, Lim J, Soohoo C, Finn G, Balastik M, Pastorino L, Wulf G, Zhou XZ, Lu KP. 2009. Essential role of Pin1 in the regulation of TRF1 stability and telomere maintenance. Nat Cell Biol 11(1):97-105.

Liou YC, Zhou XZ, Lu KP. 2011. Prolyl isomerase Pin1 as a molecular switch to determine the fate of phosphoproteins. Trends Biochem Sci 36(10):501-514.

Liu Y, Wang X, Sun CY, Wang J. 2015. Delivery of mitogen-activated protein kinase inhibitor for hepatocellular carcinoma stem cell therapy. ACS Appl Mater Interfaces 7(1):1012-1020.

Malone RW, Felgner PL, Verma IM. 1989. Cationic liposome-mediated RNA transfection. Proc Natl Acad Sci U S A 86(16):6077-6081.

Mandal B, Bhattacharjee H, Mittal N, Sah H, Balabathula P, Thoma LA, Wood GC. 2013. Core-shell-type lipid-polymer hybrid nanoparticles as a drug delivery platform. Nanomedicine 9(4):474-491.

Mantovani F, Tocco F, Girardini J, Smith P, Gasco M, Lu X, Crook T, Del Sal G. 2007. The prolyl isomerase Pin1 orchestrates p53 acetylation and dissociation from the apoptosis inhibitor iASPP. Nat Struct Mol Biol 14(10):912-920.

Morris MC, Depollier J, Mery J, Heitz F, Divita G. 2001. A peptide carrier for the delivery of biologically active proteins into mammalian cells. Nat Biotechnol 19(12):1173-1176.

Nakamura Y, Tensho K, Nakaya H, Nawata M, Okabe T, Wakitani S. 2005. Low dose fibroblast growth factor-2 (FGF-2) enhances bone morphogenetic protein-2 (BMP-2)-induced ectopic bone formation in mice. Bone 36(3):399-407.

Park OJ, Kim HJ, Woo KM, Baek JH, Ryoo HM. 2010. FGF2-activated ERK mitogen-activated protein kinase enhances Runx2 acetylation and stabilization. J Biol Chem 285(6):3568-3574.

Raemdonck K, Braeckmans K, Demeester J, De Smedt SC. 2014. Merging the best of both worlds: hybrid lipid-enveloped matrix nanocomposites in drug delivery. Chem Soc Rev 43(1):444-472.

Ryo A, Suizu F, Yoshida Y, Perrem K, Liou YC, Wulf G, Rottapel R, Yamaoka S, Lu KP. 2003. Regulation of NF-kappaB signaling by Pin1-dependent prolyl isomerization and ubiquitin-mediated proteolysis of p65/RelA. Mol Cell 12(6):1413-1426.

Ryoo HM, Lee MH, Kim YJ. 2006. Critical molecular switches involved in BMP-2-induced osteogenic differentiation of mesenchymal cells. Gene 366(1):51-57.

Shen ZJ, Hu J, Ali A, Pastor J, Shiizaki K, Blank RD, Kuro-o M, Malter JS. 2013. Pin1 null mice exhibit low bone mass and attenuation of BMP signaling. PLoS One 8(5):e63565.

Vaishya R, Khurana V, Patel S, Mitra AK. 2015. Long-term delivery of protein therapeutics. Expert Opin Drug Deliv

12(3):415-440.

Wang X, Kluge JA, Leisk GG, Kaplan DL. 2008a. Sonication-induced gelation of silk fibroin for cell encapsulation. Biomaterials 29(8):1054-1064.

Wang X, Yucel T, Lu Q, Hu X, Kaplan DL. 2010. Silk nanospheres and microspheres from silk/pva blend films for drug delivery. Biomaterials 31(6):1025-1035.

Wang Y, Rudym DD, Walsh A, Abrahamsen L, Kim HJ, Kim HS, Kirker-Head C, Kaplan DL. 2008b. In vivo degradation of three-dimensional silk fibroin scaffolds. Biomaterials 29(24-25):3415-3428.

Yan M, Du J, Gu Z, Liang M, Hu Y, Zhang W, Priceman S, Wu L, Zhou ZH, Liu Z, Segura T, Tang Y, Lu Y. 2010. A novel intracellular protein delivery platform based on single-protein nanocapsules. Nat Nanotechnol 5(1):48-53.

Yan S, Zhang Q, Wang J, Liu Y, Lu S, Li M, Kaplan DL. 2013. Silk fibroin/chondroitin sulfate/hyaluronic acid ternary scaffolds for dermal tissue reconstruction. Acta Biomater 9(6):6771-6782.

Yang Y, Niu Y, Zhang J, Meka AK, Zhang H, Xu C, Lin CX, Yu M, Yu C. 2015. Biphasic Synthesis of Large-Pore and Well-Dispersed Benzene Bridged Mesoporous Organosilica Nanoparticles for Intracellular Protein Delivery. Small 11(23):2743-2749.

Yasuda K, Ogawa Y, Yamane I, Nishikawa M, Takakura Y. 2005. Macrophage activation by a DNA/cationic liposome complex requires endosomal acidification and TLR9-dependent and -independent

pathways. J Leukoc Biol 77(1):71-79.

Yoon WJ, Cho YD, Kim WJ, Bae HS, Islam R, Woo KM, Baek JH, Bae SC, Ryoo HM. 2014. Prolyl isomerase Pin1-mediated conformational change and subnuclear focal accumulation of Runx2 are crucial for fibroblast growth factor 2 (FGF2)-induced osteoblast differentiation. J Biol Chem 289(13):8828-8838.

Yoon WJ, Islam R, Cho YD, Ryu KM, Shin HR, Woo KM, Baek JH, Ryoo HM. 2015. Pin1 plays a critical role as a molecular switch in canonical BMP signaling. J Cell Physiol 230(3):640-647.

Yoon WJ, Islam R, Cho YD, Woo KM, Baek JH, Uchida T, Komori T, van Wijnen A, Stein JL, Lian JB, Stein GS, Choi JY, Bae SC, Ryoo HM. 2013. Pin1-mediated Runx2 modification is critical for skeletal development. J Cell Physiol 228(12):2377-2385.

V. Conclusion

These results show that Fibroplex can be fabricated with natural silk fibroin protein and clinically applicable cationic lipids to achieve high intracellular delivery efficiency with enhanced capacity and stability. Fibroplex showed supreme biocompatibility and protected cargos from being damaged during endocytosis, enabling the stable, long-term, intracellular release and activity of cargos. As a result, more therapeutic proteins could be delivered into cells, and the successful delivery of functional proteins into tissues in vivo suggests the possibility of using Fibroplex for delivering protein drugs in clinical applications.

Fibroplex provides an alternative method for delivering proteins more effectively. We were able to deliver various proteins into skin tissue, and we observed long-term, stable protein delivery followed by protein activation, which could facilitate the application of therapeutic proteins in treating hereditary diseases or cancer. As such, we expect that by modifying the cationic lipids with disease-specific ligands[32], we will be able to deliver proteins into specific target tissues or cells and deliver multiple proteins that simultaneously regulate cellular functions. Such a novel intracellular protein delivery system will provide opportunities for the use of protein drugs in cellular imaging applications and in therapies for cancer and hereditary disorders.

In Part II, these data demonstrate that direct delivery of

recombinant Pin1 via fibroin nanoparticle encapsulated cationic lipid complex successfully maintain functional interaction with Runx2 or Smad1/5 and enhances canonical BMP2 signaling and is crucial for BMP2-induced osteogenic differentiation. Therefore, we suggest here that direct delivery of modifying enzymes, such as Pin1, might represent valuable protein drug to correct abnormal Runx2 activity and to ensure the optimal fate determination of osteogenic cells in the differentiation and development of bone.

국문초록

피브로인-양전하 지질 복합체를 이용한 단백질의 세포 내 전달 방법에 대한 연구

김 우 진

서울대학교 대학원

치의과학과 분자유전학전공

(지도교수 류 현 모)

연구목적: 치료용 단백질을 세포 내로 직접 전달하는 것은 유전자 또는 단백질 기능이상과 관련된 난치성 질환의 극복을 위해 매우 효과적인 방법이다. 그러나, 생체 거대 분자로서 단백질은 큰 사이즈와 다양한 전기적 성질 때문에 세포막을 통과하여 세포 내로 직접 전달하는 것이 매우 큰 기술적 난점으로 지적되고 있다. 생체적합성이 높고, 생분해성이 있어 장기간 안정적인 약물 방출양상을 보이는 실크 피브로인 나노 입자는 세포 내 장기간 치료용 약물을 안정적으로 전달하는데 최적화 된 단백질 약물 전달체이나, 나노 입자를 구성하는 피브로인 단백질의 특성 상 입자 전하가 높은 음전하를 띠고 있어 세포막을 통해 세포 내 도입되는 것이 매우 어렵다. 이러한 한계의 극복을 위해, 높은 음전하를 보상하는 양전하 지질과 나노 입자의 복합체를 형성하여 높은 효율로 세포

내 단백질을 전달하고, 장기간 안정적으로 단백질 약물을 방출 할 수 있는 새로운 실크피브로인 나노입자-양전하 지질 복합 단백질 약물 전달체를 개발하고 이의 특성과 효과를 연구하였다.

연구방법: 실크 피브로인 단백질 수용화 용액을 이용하여, 모델 단백질 약물로서 GFP, HRP, Tyrosinase 그리고 Luciferase를 도입시킨 나노 입자를 제작한 다음, 이의 표면전하의 개선을 위하여 DOTAP:DOPE 양전하 지질과 복합체를 형성하였다. 복합체의 특성의 규명을 위하여 주사 전자 현미경, 투과 전자현미경, 컨포컬 레이저 현미경을 통해 관찰하였으며, 크기 및 전기적 특성 분석을 위하여 제타-사이저를 통해 측정하였다. 단백질 약물의 도입효율과 방출 양상은 ELISA를 통해 측정하였으며, 세포 독성의 관찰을 위하여 다양한 농도에서 MTT 어세이를 실시하였다. 도입된 모델 단백질의 세포 내 효과를 확인하기 위하여, 효소 활성도를 측정하였으며, In-vivo 도입 효과를 확인하기 위하여 피부 멜라닌 축적 유도 및 흑색피부종 암세포를 유도한 다음 암의 크기 감소를 확인하였다.

결과: 실크 피브로인 나노 입자-양전하 지질 복합체는 다양한 종류의 세포에 90% 이상의 높은 효율로 단백질을 전달하였으며, 세포 내에 도입된 이후 10일 이상 안정적으로 약물을 방출하고, 도입된 약물은 안정적인 효과를 나타내었다. 세포 및 생체에 있어서 실크 피브로인-양전하 복합체의 독성은 일반 양전하 지질 리포좀

과 비교하여 현저하게 낮게 나타났으며, 도입된 단백질에 의한 ER stress 도 나타나지 않았다. 동물 모델에서 상기 복합체는 HRP, GFP, Tyrosinase를 피부 조직에 성공적으로 전달하여, 각 단백질 약물의 기능 발현을 통해 멜라닌 축적 또는 흑색피부종의 체적 감소 효과를 보였다. 그 결과, 실크 피브로인 나노입자-양전하 지질 복합체는 높은 효율로 세포에 단백질 약물을 전달하는데 효과적인 약물 전달 시스템으로 활용될 수 있을 것으로 기대된다.

주요어 : 실크 피브로인, 나노 입자, 나노입자-양전하 지질 복합체, 단백질 약물

학 번 : 2008-22062